ISTANBUL TECHNICAL UNIVERSITY ★ GRADUATE SCHOOL OF SCIENCE ENGINEERING AND TECHNOLOGY

EXPERIMENTAL INVESTIGATION OF A SINGLE SPANWISE VORTEX GUST IMPINGING ON A RECTANGULAR WING

M.Sc. THESIS

Kader ENGİN

Department of Aeronautics and Astronautics Engineering

Aeronautics and Astronautics Engineering Programme

ISTANBUL TECHNICAL UNIVERSITY ★ GRADUATE SCHOOL OF SCIENCE ENGINEERING AND TECHNOLOGY

EXPERIMENTAL INVESTIGATION OF A SINGLE SPANWISE VORTEX GUST IMPINGING ON A RECTANGULAR WING

M.Sc. THESIS

Kader ENGİN
(511161176)

Department of Aeronautics & Astronautics Engineering

Aeronautics & Astronautics Engineering Programme

Thesis Advisor: Prof. Dr. Nuriye Leman Okşan ÇETİNER YILDIRIM

ISTANBUL TEKNİK ÜNİVERSİTESİ ★ FEN BİLİMLERİ ENSTİTÜSÜ

AÇIKLIK BOYUNCA UZANAN TEKİL BİR GİRDAP SAĞANAĞIN DİKDÖRTGEN PLATFORMA SAHİP KANAT İLE ETKİLEŞİMİNİN DENEYSEL İNCELENMESİ

YÜKSEK LİSANS TEZİ

Kader ENGİN
(511161176)

Uçak ve Uzay Mühendisliği Anabilim Dalı

Uçak ve Uzay Mühendisliği Programı

Tez Danışmanı: Prof. Dr. Nuriye Leman Okşan ÇETİNER YILDIRIM

Kader Engin, a M.Sc. student of İTU Graduate School of Science Engineering and Technology student ID 511161176, successfully defended the thesis entitled "EXPERIMENTAL INVESTIGATION OF A SINGLE SPANWISE VORTEX GUST IMPINGING ON A RECTANGULAR WING", which she prepared after fulfilling the requirements specified in the associated legislations, before the jury whose signatures are below.

Thesis Advisor : **Prof. Dr. Okşan ÇETİNER YILDIRIM** ....
Istanbul Technical University

Jury Members : **Dr. Hayri ACAR** ....
Istanbul Technical University

Prof. Dr. S. Kunt ATALIK ....
Boğaziçi University

Date of Submission : 04 May 2020
Date of Defense : 03 June 2020

To my family and friends,

FOREWORD

First of all, I would like to express my gratefulness to Trisonic Family. My thesis advisor Prof. Dr. N. L. Okşan Çetiner Yıldırım for her guidance and support during the development of this thesis. And to Murat Sarıtaş, Onur Son, İdil Fenercioğlu, Hasan Tabanlı and Aliosman Tabanlı for their support and friendship.

I am also thankful to Egemen Aydın, Cansu Uzay, Ezgi Ede for their valuable friendship and support. But most importantly, helping me against all the negativeness and stress of my school years.

And the last but most importantly, I would like to express my gratitude to my family for their great support and encouragements. I would not be able to be at where I am without their love, efforts and guidance.

June 2020 Kader ENGİN

TABLE OF CONTENTS

Page

ABBREVIATIONS

AoA	**:** Angle of Attack
DPIV	**:** Digital Partical Image Velocimetry
MAV	**:** Micro Aerial Vehicle
PSP	**:** Polyamide Seeding Particle
Re	**:** Reynolds Number

SYMBOLS

C_d	: Drag Coefficient
C_l	: Lift Coefficient
t	: Time
α	: Angle of attack
α_{eff}	: Effective angle of attack
AR_{eff}	: Effective aspect ratio

LIST OF TABLES

Page

LIST OF FIGURES

Page

EXPERIMENTAL INVESTIGATION OF A SINGLE SPANWISE VORTEX IMPINGING ON A RECTANGULAR WING

SUMMARY

The aim of this study is to investigate the effects of a single spanwise vortex impingement on flow structures around and loading on a rectangular wing. An experimental approach is adopted to investigate by gathering force data from the wing and visualization of flow structures with DPIV technic.

The experiments are conducted in the large scale water channel located in Trisonic Laboratory of Istanbul Technical University's Faculty of Aeronautics and Astronautics. A Reynolds Number of 10.000 is chosen for all experiments which corresponds to U_{∞} = 0.1 m/s. A flat plate upstream of the model undergoing clockwise 180 degree turn is used for the generation of a single vortex and the vortex impacts a stationary rectangular flat plate wing with AR_{eff}= 4 located downstream of the vortex generator. Forces acting on the model during experiments are acquired by a force/torque sensor. Simultaneously, flow structures around the wing are captured by a DPIV system during vortex impingement.

The mounting arrangements of the gust generator and the wing, are such that both are able to do pitch and plunge motions. A total of 7 different angle of attack values for the stationary wing and 3 different offsets only varying in y-axis for the gust generator with respect to model to change the vortex path are combined to generate 21 test cases of this study.

The difference in wing loading due to the vortex impingement for various angle of attack values are compared for the same offset value. Likewise, they are compared when only the gust generator offset changes and angle of attack of the model is kept the same. Following this procedure, images gathered by DPIV system are investigated in conjunction with the force data. The general trend of the aerodynamic forces acting on the model due to vortex impingement shows agreement with the literature work on the subject. Drag coefficient is less affected by the vortex impingement especially when the model has a high angle of attack. However, the lift coefficient shows that as

the angle of attack value increases, the effect of the vortex impingement on lift becomes drastic. The wing loading is correlated with the effective angle of attack calculated quarter chord upstream of the leading edge using the quantitative velocity field obtained using the DPIV system. The study actually mimics a transient vortex gust encounter. The strength and width of the gust is also determined using the DPIV images. Although the impinging vortex is the same for all cases investigated, the offset value and the angle of attack affect the vortex trajectory and therefore wing loading.

AÇIKLIK BOYUNCA UZANAN TEKİL BİR GİRDAP SAĞANAĞIN DİKDÖRTGEN PLATFORMA SAHİP KANAT İLE ETKİLEŞİMİNİN DENEYSEL İNCELENMESİ

ÖZET

Atmosferdeki akışın dengesiz doğası, havacılık tarihi boyunca bir zorluk oluşturmaktadır. Son zamanlarda, insanlar hava araçlarının sınırlarını zorlamaya başladıkça ve yeni görev türleri ortaya çıktıkça, kararsız akış koşullarını anlamak daha fazla önem kazanmıştır. Gözetleme veya keşif gibi mevcut görevler, mikro veya insansız hava araçlarının daha küçük olmasını, düşük rakımlarda veya diğer yapıların iz bölgesinde çalışmalarını gerektirir. Sayılan faktörlerin bileşimi hava araçlarının büyük ölçekli sağanaklar ile karşılaşma potansiyelini arttırırken aynı zamanda bu karşılaşmalara karşı daha duyarlı olmalarına sebep olur. Bu nedenle sağanakların kanat yüklemesine etkilerinin araştırılması önem teşkil etmektedir.

Bu çalışmanın amacı, açıklık boyunca uzanan bir tekil girdabın akış yapıları ve kanada binen aerodinamik yükler üzerindeki etkilerini araştırmaktır. Bu şekilde bir girdap sağanağın sabit bir kanatta yaratacağı sonuçlar incelenecektir. Dijital Parçacık Görüntüleme Hızölçeri sistemi ile akış yapılarını görüntüleyerek ve bir kuvvet/tork sensörü kullanımıyla modelden kuvvet bilgisini edinerek konuya deneysel bakış açısıyla yaklaşılmıştır.

Deneyler, İstanbul Teknik Üniversitesi, Uçak ve Uzay Bilimleri Fakültesi, Trisonik Laboratuvarı'nda bulunan geniş ölçekli su kanalında gerçekleştirilmiştir. Deneylerde Reynolds Sayısı 10 000 olarak seçilmiştir ve bu sayı deney koşullarında serbest akış hızının 0.1 m/s olmasına karşılık gelmektedir. 10 cm veter ve 40 cm kanat açıklığına sahip bir plaka sağanak jeneratörü olarak kullanılmak üzere akışla önce karşılaşacak şekilde yerleştirilir. Bu düzeneğin ardına ise bağlantı kirişine kuvvet sensörü monte edilmiş, 10 cm veter ve 20 cm kanat açıklığına sahip plaka model olarak yerleştirilir. İki düzenek de kanat bağlantı kirişlerine monte edilmiş olan yunuslama motoru yardımıyla yunuslama hareketi yapabilmektedir. Kanatların yunuslama motoruyla birlikte bağlı olduğu lineer tabla (linear table) ise akışa dik yönlü hareket yapılmasını

sağlamaktadır. Bu şekilde bir vortex sağanağın sabit bir kanatta yaratacağı sonuçlar incelenecektir.

Girdap, sağanak jeneratörünün saat yönünde 180 derece dönüşünü sabit açısal hızda 4 saniyede tamamlaması ile oluşturulur. Oluşumunun ardından söz konusu girdap sağanak jeneratörünün ardında yer alan sabit hücum açısındaki model ile etkileşir. Bu etkileşim sonucunu araştırmak amacıyla modelin 7 farklı hücum açısı ve sağanak jenöratörünün 3 farklı düşey konum kombinasyonundan oluşan 21 deney durumu belirlenmiş ve kullanılmıştır.

Deney sırasında inceleme alanındaki akış yapıları Dijital Parçacık Görüntüleme Hızölçeri (DPGH) sistemi tarafından yakalanır. Bu sistemde akışkana polimer parçacıklar karıştırılarak akış tohumlanır ve düzlemsel lazer ile akış alanının aydınlatılmasıyla parçacıklar görünür hale gelir. Anlık olarak akış alanı fotoğraflanır ve DPGH programı fotoğraflardaki parçacık hareketinden yola çıkarak akış alanında hız vektörlerini hesaplar. Bu aşamanın ardından veri işlemede laboratuvarın kurum içi kodu kullanılarak filtreleme ve maskeleme yapılır.

Sağanak ile etkileşim sırasındaki inceleme alanındaki akış yapıları Dijital Parçacık Görüntüleme Hızölçeri sistemi tarafından yakalanırken, kuvvetler eş zamanlı olarak model kirişine monte edilmiş bir kuvvet / tork sensörü ile alınır. Kuvvet/tork sensöründen alınan ölçümler filtrelenip gürültüden arındırılmasının ardından taşıma ve sürükleme katsayılarının hesaplanmasında kullanılır.

Veri işlemenin ilk adımlarından biri kanada etki eden sağanağı karakterize etmektir. Bu işlem literatürde yapılan araştırmalar ile ortak bir dil kurulmasına ve karşılaştırma yapılmasına olanak sağlar. Deneyde sağanak jeneratörü tarafından oluşan girdabın t=8 s anında hız vektörlerine bakılarak bu işlem gerçekleştirilmiştir. Sonuç olarak Sağanak Oranı (Gust Ratio) yaklaşık 1.0, Sağanak Genişliği (Gust Width) ise 0.4 bulunmuştur.

Aynı sağanak jeneratörü pozisyonu için taşıma ve sürükleme katsayısı karşılaştırılmıştır. Burada sağanağın oluşturduğu farka bakılmıştır.

Taşıma katsayısı değişimlerindeki genel eğilim, deneylerin çoğu için benzerlik göstermektedir. İlk başta, kanat üzerinde etkili olan kuvvetler stabil durumdadır. Ardından, sağanak jeneratörü hareketinin başlamasıyla ilişkili olarak t = 5 s'den sonra lokal bir maksimum gözlenir. Görülen bu lokal ekstremiteyi, t = 8 s civarında bir minimum uç nokta izler. Bunu takiben kuvvetlerin toparlanma süreci başlar ve bir başka lokal maksimum tepe noktası gözlenir. Son olarak, taşıma katsayısı baştaki stabil durum değeri etrafında salınım yapar.

Benzer şekilde, sürükleme katsayısı değişimi de deneylerde benzerlik gösterir. Sağanak jeneratörü hareketine başlamadan önce, eğriler stabil değerleri etrafında dalgalanır. Hareket t = 5 s'de başladığında, bir minimum lokal pik ardından bir ekstrem maximum pik gözlenir. Bu piklerin zamanlamasının taşıma katsayısı değişimlerindeki piklerin zamanlamasıyla eşleşmektedir, ancak eğimleri zıttır. Daha sonra kuvvetler toparlanmaya başlar ve başka bir yerel minimum gözlenir. Son olarak, kuvvetler sağanak jeneratörünün hareketinden önceki değerler etrafında dalgalanır ve sabit duruma ulaşır.

Girdap etkileşimi nedeniyle modele etki eden aerodinamik kuvvetlerin genel eğilimi benzerlik gösterse de hücum açısıyla ilişkili olarak lokal pik değerlerinde farklılıklar gözlenmektedir. Sürükleme katsayısı değişimlerinin sonuçları, model daha yüksek hücum açısı değerine sahip olduğunda girdap karşılaşmasından daha az etkilendiğini göstermektedir.

Dijital Parçacık Görüntüleme Hızölçeri sisteminden elde edilen akış yapısı görüntüleri de kuvvet verileriyle birlikte incelenmektedir. Sağanak jeneratör hareketi başlamadan önce kuvvetler stabil değerlerindedir ve akış alanı herhangi bir büyük girdap yapısından yoksundur. Sağanak jeneratörü ilk hareketi sırasında bir küçük pozitif girdap yaratır ve bu da katsayı değişimlerindeki ilk lokal uç noktanın oluşmasında etkilidir. Ardından güçlü bir negatif girdap akış alanına girer. Negatif girdap yoluna devam ettikçe, modelin ön kenarında bir tepki olarak pozitif girdap oluşmaya başlar. Bu noktada hem taşıma hem de sürükleme katsayısı değişimleri sırasıyla ekstrem bir uç nokta değerlerine ulaşır. Pozitif hücum kenarı girdabı modelden kopar ve negatif girdapla etkileşir. Sonuç olarak, her iki girdabın da akış alanındaki etkileri nötralize edilir ve kuvvetler bu zaman aralığında toparlanır. Bu proses deneylerin tamamında benzer bir şekilde ilerlemektedir. Ancak, girdabın yörüngesine ve kanadın hücum açısına bağlı akış alanında oluşan yapıların zamanlamalarında ve şiddetlerinde farklılıklar gözlenmiştir.

Kanat yükü, DPGH sistemi kullanılarak elde edilen hız alanı verileri kullanılarak hücum kenarının çeyrek veter ilerisinde hesaplanan efektif hücum açısı ile ilişkilidir.

1. INTRODUCTION

Unstable nature of flow in the atmosphere present a challenge throughout the history of aviation. Recently, understanding various unsteady flow conditions gained more importance as humans started to push boundaries of aerial vehicles and new type of mission opportunities arised. Current missions such as survaillance or reconnaiscence, require micro or unmanned air vehicles to be smaller, operate in low altitudes or in the wakes of other structures which makes them susceptible to gust encounters. Watkins et al. (2006) states that neutralizing effects of unpredictable pitch and roll introductions produced by small eddies or vortices as a result of turbulence is the greatest concern for these air vehicles. For these reasons, researchers diverted their attention to unsteady gust-wing interaction to have a better understanding of effects on wing loading and how to eliminate these unpredictable effects.

This study presents a view to gust-wing interaction by focusing on the effects of singular spanwise vortex impingement on flow structures and wing loading. The gust generated upstream of flow impinges on a model which remains at constant angle of attack through experiments. The model is kept at 7 different angles of attack and the gust is generated at 3 coordinates only varying in y axis to have a better understanding of the phenomena. Although the offset of gust generator changes, gust width and strength does not vary in experiments. During these 21 test cases, simultaneous Digital Particle Image Velocimetry (DPIV) and force measurements are obtained. Then, force measurements are used to calculate aerodynamic coefficients. DPIV data is processed by an in-house code and processed data is used for visualizing flow structures and calculating effective angle of attack.

The following chapters gives information about literature, experimental setup, results and conclusions respectively. In Chapter 2, researches about gust generation methods and gust-wing interaction are summarized. In Chapter 3, detailed description of the experimental setup is given in terms of the flow system, test model, motion system, force measurement and DPIV. Following chapter starts with the information about test cases, continues with characterization of gust and results based on the post processed data. Finally, concluding remarks and recommendations for further studies are given in Chapter 5.

2. LITERATURE OVERVIEW

Several studies has been conducted about gust generation and gust-wing interaction since the need for eliminating unpredictable effects of unsteadiness arised. These studies can be divided to 3 categories depending on the type of gust encounter as shown in Figure 2.1 below.

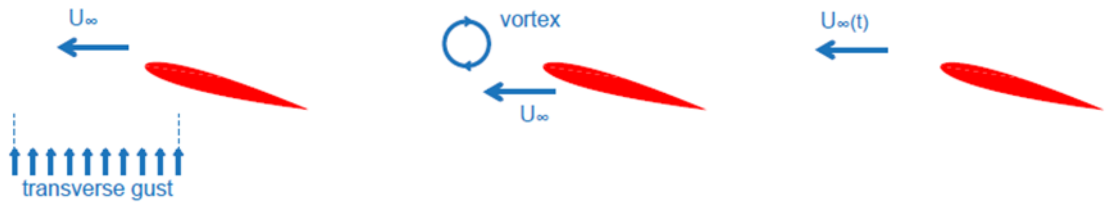

(a) Transverse Gust **(b) Vortex Gust** **(c) Streamwise Gust**

Figure 2.1 A schematic of gust encounter types (Jones, 2020)

A model moving through a flow field disturbed by an introduction of upwards velocity is given as an example of transverse gust encounter in Fig. 2.1(a). This type of gust is encountered as a result of athmospheric weather changes and in the form of large scale wakes due to terrain, large buildings or naval ships (Jones and Çetiner, 2020). Fig. 2.1(b) showes a vortex gust in a flow field with constant free stream velocity for a wing kept at constant angle of attack. Examples of this type of gust can be listed as follows: wakes of other wings such as in the case of rotorcraft or wind turbines, wakes of large structures such as buildings or ships and athmospheric or seabed turbulence. Fig. 2.1(c) demonstrates a wing kept at constant angle of attack in a flow field where streamwise velocity is a function of time. This type of gust is encountered at lifting surfaces in tides and rotorcrafts.

2.1 Transverse Gust Researches

Several studies on transverse gust from experimental and numerical perspective were made. Experimental study of transverse gust researches was conducted by Corkery et al. (2018) and the results were compared with Küssner function predictions. A pump and a duct system were used as gust generator to produce a top hat shaped gust in a tow tank. PIV data and force measurements were collected during passage of a flat plate with 0 degree of AoA. As a result, C_l from force measuments agreed with predictions of Küssner function. Also, formation of a strong leading edge vortex associated with peak of forces observed during the entry of model to the gust field.

Later, Moushegian and Smith (2019) used Delayed Detached Eddy Simulation to analyze response of a wing encountering a two chord length top hat gust and compared results with both experimental and Küssner function predictions. As a result of increased gust ratio, Küssner function was not able to predict the behavior. However, the numerical analysis fit well with the experimental results.

The effect of gust ratio and the AoA of model during the transverse gust encounter was studied by Biler et al. (2019). Experiments were conducted in a tow tank with water jet assembly as a gust generator. Resultant sine square wave profiled gust's velocity was adjusted to study various gust ratios. Additionally, several cases with different AoA were chosen to investigate the effect of AoA. According to this study, an increment in gust ratio caused both lift and drag coefficients to have higher maximum values. However, raising angle of attack affected these coefficients up to a limit of 20 degree. When a comparison for the cases with same effective angle of attack had been made, a similarity of results was observed which indicated that the gust encounter was dependent on the effective AoA and not the on gust ratio or the geometric AoA. Field Velocity Method was also applied as a numerical simulation of the flow and forces obtained from computational analysis agreed with experimental ones.

2.2 Vortex Gust Researches

The first priority for the experimental studies for this type of gust was the gust generation, since creating smooth vortices with appropriate velocity profiles was a challenge itself. The experiments conducted by Wei et al. (2019) showed that a simple wing undergoing plunging and pitching motions was enough to create a sinusoidal gust. Another vortex gust generation method in experiments was placing a rotating cylinder in the upstream flow and the model was subjected to Von Karman vortices shed from the cylinder which was implemented by Medina et al. (2019). After introduction of these methods researchers diverted their attention to study the effects of wing-vortex interactions.

Hufstedlar and McKeon (2019) experimentally studied methods for gust generation and gust-wing interaction at Re=20000. Two different methods for generation of a singular transverse vortex was investigated; a pitching airfoil and a plunging airfoil changing its direction to generate gust. As the vortex passed through the gust, a steep decrease accompanied by an increase was observed in lift coefficient. Also, increase of AoA delayed recovery of forces for cases with higher AoA. The results were not affected by the method of gust generation. (Hufstedlar and McKeon , 2019).

Another study by Hahn et al. (2013) focused on the effects of vortex gusts on an airfoil with a flap. Experiments were conducted in a wind tunnel with an airfoil upstream to generate quasi-two dimensional vortices. They found that the airfoil's leading edge was sensitive to changes in the induced angle of attack associated with gust generation rather than geometric angle of attack similar to the results of the transverse gust study of Biler et al. However, leading edge of the flap was affected by positive velocity in streamwise direction induced by the vortex.

A study by Barnes and Visbal (2017) focused on the numerical simulation of vortex gust-wing encounter by using high fidelity LES method. A Taylor vortex introduced to flow field with varying vertical positions while a NACA 0012 airfoil was kept at 4 degree of AoA downstream. According to this research, lift coefficient became more affected by the gust as the vortex was introduced in line with the leading edge of model in comparison with other cases with an offset. When the gust was offset up and down 0.25 c from the chord line, flow structures were found to be similar. However, the strength of flow structures was affected.

2.3 Streamwise Gust Researches

The method of generation of streamwise gusts in water was moving model instead of changing the free stream velocity. Mulleners et al. (2017), conducted experiments in a tow tank with an acceleration mechanism for the wing to study effects of the streamwise gust. First set of experiments included a wing's transition from inial state to U_0 =0.3 m/s with a constant acceleration and an angle of attack of 30 degree during travel of one chord length. These motion were repeated several times to reach fully developed flow. Then the wing was accelerated from U_0 to $1.5U_0$ to generate streamwise gust for a second set of experiments. It is found that the redevelopment of stall was characterized by shedding of vortices from the wing and the process was similar for both of cases. A decrease was also observed in the lift coeffient associated with the shedding of vortices.

3. EXPERIMENTAL SETUP

This section consist of detailed description of the elements that make up the experimental setup used in the thesis. These elements are flow system (water channel), test model, motion system, force measurement and DPIV system.

3.1 Flow System (Water Channel)

The experiments are conducted in free surface, closed circuit, large scale water channel located in Trisonic Laboratory of Istanbul Technical University's Faculty of Aeronautics and Astronautics. The water channel consists of various parts to provide better flow conditions for experiments. First, regular city water passes through carbon and propylene sediment filters for decontamitanion from particles which is especially important to get better results when using DPIV. Then, water is directed to settling chamber by a centrifugal pump system. Before arriving in the test section, filtered water passes through several honeycomb and screen arrangements to decrease turbulent intensity. After this process, water arrives in a 2:1 contraction section to be accelerated into the test section. The test section is made of transparent acrylic glass to allow the use of DPIV and LDA measurements. Dimensions of this section is 927 mm x 750 mm which can be seen in Figure 3.1. Flow velocity in test section can be adjusted from 0 to 140 mm/s by an ABB AC Drive. Flow velocity is determined as 0.1 m/s to reach a Reynolds Number of 10 000 and this velocity is used during all the experiments.

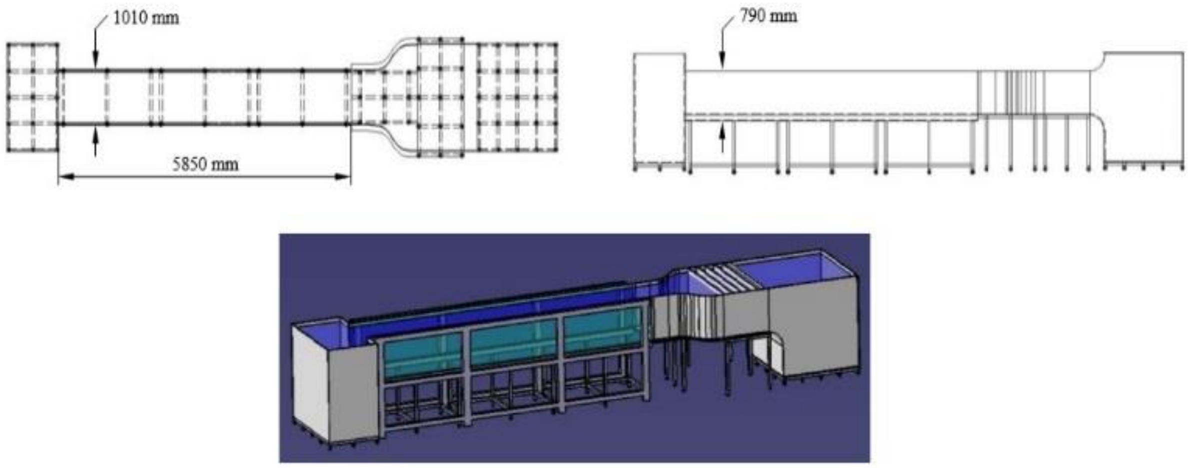

Figure 3.1 : Schematics of the water channel (Fenercioglu, 2010)

3.2 Test Model

A flat plate with a 10 cm chord and 40 cm span is mounted from its mid-chord to be used as a gust generator upstream. At downstream, a flat plate with 10 cm chord and 20 cm span flat plate is mounted from its leading edge to study the effects of the single spanwise vortex, Figure 3.2 visualize this experimental setup. Both of the plates are manufactured from plexiglass to allow measurements to be taken with DPIV.

Both of the mounting beams for the gust generator and the flat plate is connected to pitch motors which are also connected to linear tables. The pitch motor is used for changing the angle of the model and linear tables able the model to do plunging motion. These motors can be also used simultaneously, which allows plates to be moved according to specified cases.

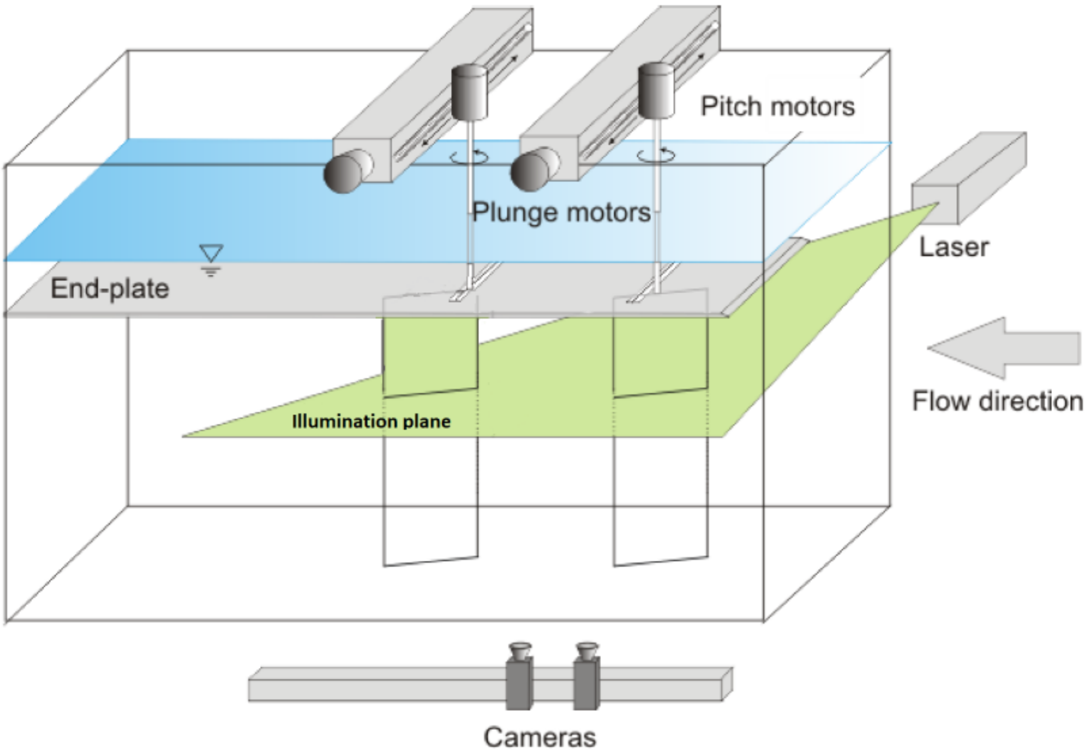

Figure 3.2 : Schematics of experimental setup

3.3 Motion System

The flat plate downstream of the flow is kept at a constant angle of attack during the experiments. However, the gust generator undergoes a ramp motion in pitching starting at t=5 s with a constant angular velocity of 45 degree per second, which ends at t=9 s. The motion signal is generated by a signal generator Labview Virtual Instrument. The synchronization of motion, force sensor and DPIV is achieved using a National Instruments PCI-6601 timer device. The pitch and plunge motions of the gust generator and the model are accomplished by Kollmorgen/Danaher Motion servo motors. These servo motors are also connected to a computer by ServoSTAR S700 digital servo amplifiers.

Figure 3.3 shows the motion signal for the gust generator and the trigger signal for data gathering systems.

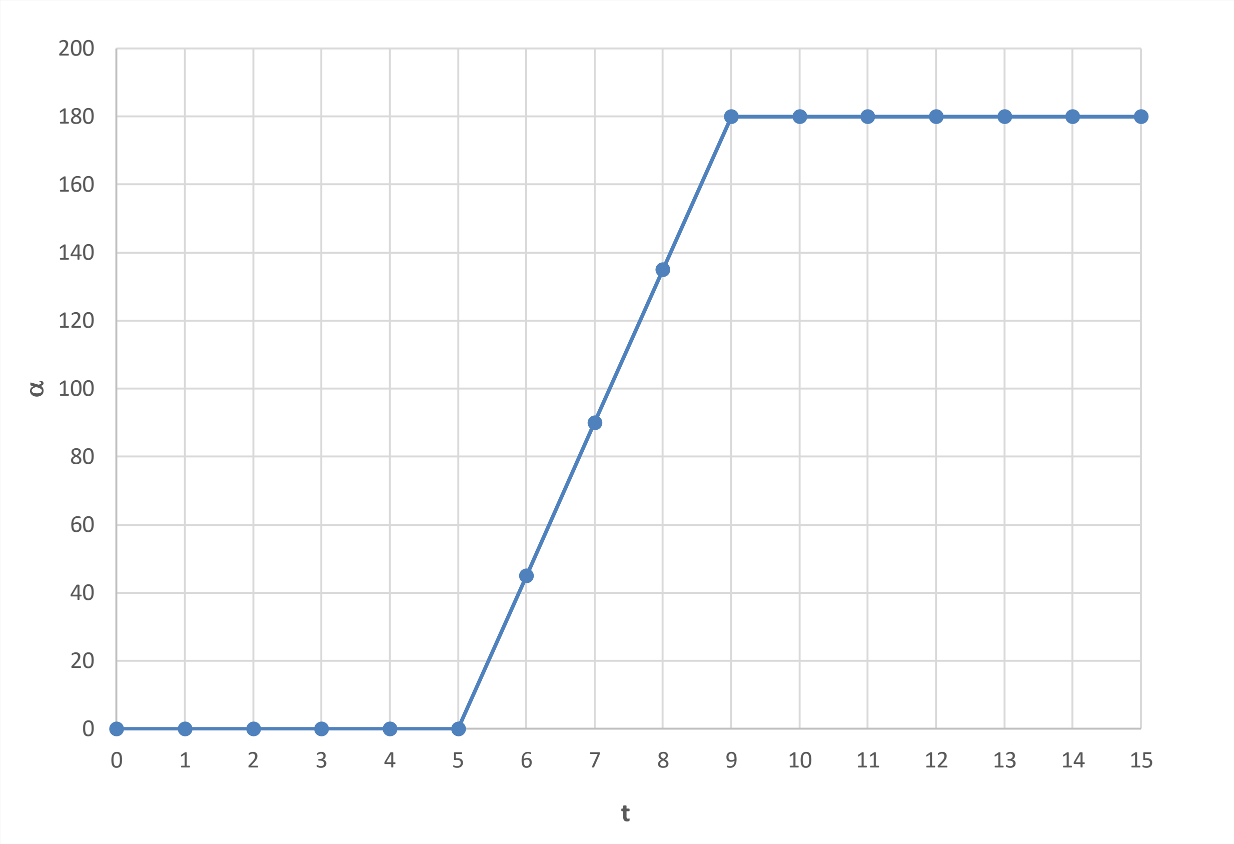

Figure 3.3: Time versus AoA of gust generator

3.4 Force Measurement

The force/torque sensor is attached to the mounting beam which is connected to the model. A six-component ATI NANO-17 IP68 Force/Torque (F/T) sensor is used for measurements with its z-axis directed normal to the pitch-plunge plane. A Labview VI is used to control the motion of the model and gathering synchronized DPIV (Digital Particle Image Velocimetry) and force measurements from the sensor.

A sampling rate of 1000 Hz is chosen for data acquisition of the sensor. An FFT (Fast Fourier Transform) Low Pass filter which allows only frequencies lower than the cut-off frequency to pass, is used to eliminate noises and mechanical vibrations. The cut-off frequency is chosen according to the motion of the gust generator since this is the source of flow disturbance. Gust generator completes its motion in 4 seconds which corresponds to 0.25 Hz in a cyclic motion case. The cut-off frequency is taken as 5 times the frequency of motion in the experiments, thus cut-off frequency is taken as 1.25 Hz.

3.5 Digital Particle Image Velocimetry

DPIV (Digital Particle Image Velocimetry) technique is used in the test section of the channel to record the quantitative flow field around the plate and therefore to analyze the vortical structures and the velocity field. The flow is illuminated by a dual cavity New Wave Solo PIV Nd-Yag laser with a maximum repetition rate of 15Hz. The maximum pulse energy is 120mJ/pulse at a wavelength of 532 nm. The flow is seeded with polyamide seeding spheres (PSP) with a mean diameter of 50 μm.

The velocity fields in the wake of the gust generator and around model are obtained using a 10-bit Dantec Dynamics Flow Sense 2M CCD camera with 1600 × 1200 pixels resolution and 35 mm diaphragm positioned underneath the water channel.

All cases have the same sampling frequency which is 8 Hz. Recorded images are interrogated using a double frame, cross-correlation technique with a window size of 64 × 64 pixels and 50% overlapping in each direction using Dantec Dynamic Studio v.6. Then an inhouse code is used for the elimination of spurious vectors and masking of the gust generator and the model.

4. RESULTS

It should be noted that although all the results will be given with a dimensional time axis, the nondimentionalization of time with convective time and chord length yields the same value as the time in seconds for all the experiments of thesis.

4.1 Test Cases

Test cases for this study are chosen in order to investigate effects of both vortex trajectory and the angle of attack of the model on loading and flow structures. Table 4.1 shows investigated test cases and their significant parameters.

	GUST GENERATOR	MODEL
Experiment No	y-coordinate offset (mm)	AoA (°)
1	19	0
2	19	5
3	19	10
4	19	15
5	19	20
6	19	30
7	19	45
8	29	0
9	29	5
10	29	10
11	29	15
12	29	20
13	29	30
14	29	45
15	39	0
16	39	5
17	39	10
18	39	15
19	39	20
20	39	30
21	39	45

Table 4.1: Test Cases

4.2 Gust Characterization

The first step of postprocess is characterizing the vortex gust impinging on the model. This analysis allows a comparison to be made with the literature work and provides an information about where this gust can be encountered. Figure 4.1 below shows the PIV images taken at t=8 s and t=8.5 s for a moderate case with following parameters: offset=29 mm and AoA=15°. The orange colored vertical and horizontal lines at the DPIV images coincide with the gust center. The next row shows u-velocity and vorticity extracted along the vertical line and plotted with respect to distance. Likewise, v-velocity is extracted along horizontal line and plotted with respect to distance along with corresponding vorticity values. A $3rd$ order polynomial is fitted to the mentioned velocity data and the polynomial is used in the calculation of gust parameters.

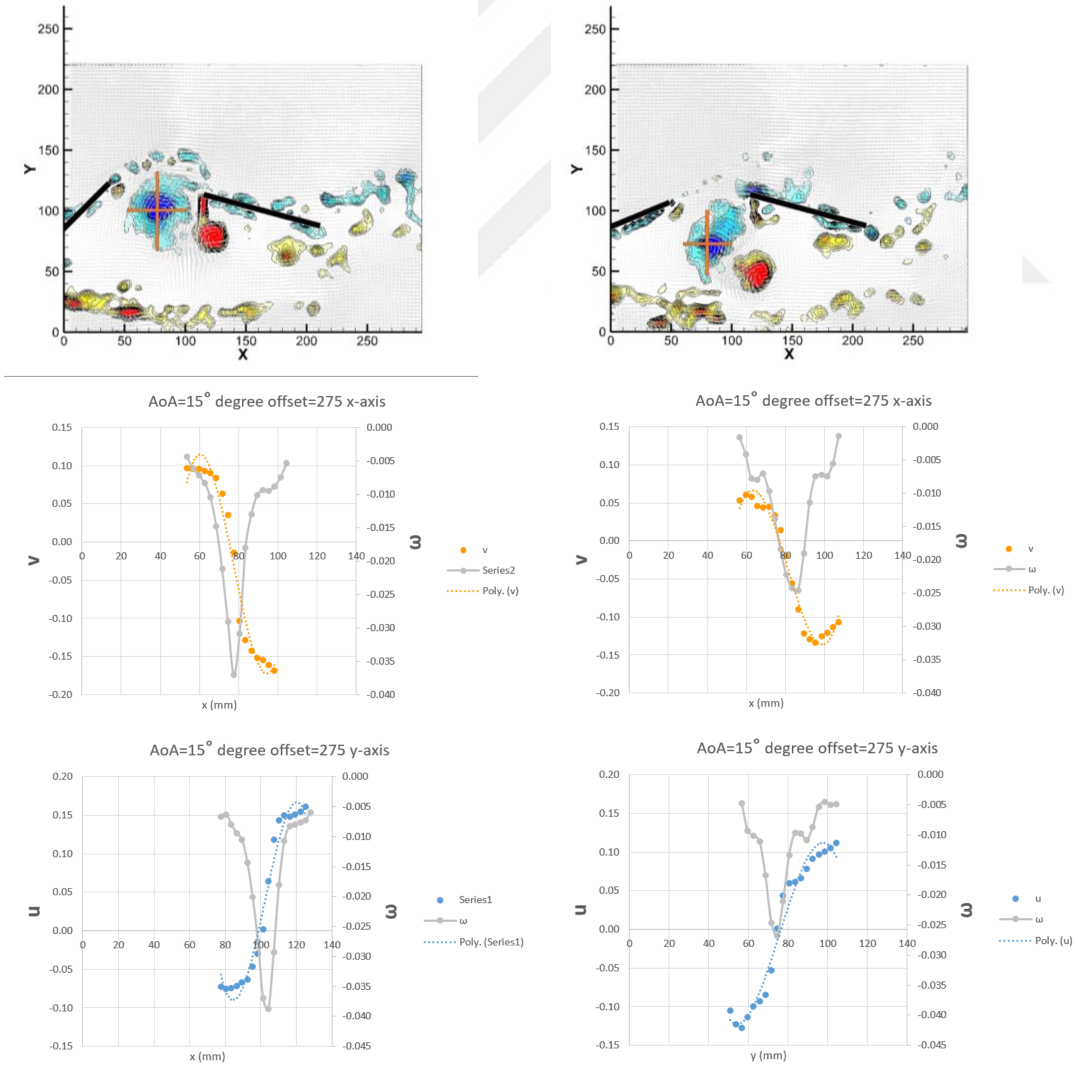

Figure 4.1: Velocity and vorticity distribution of gust for the case with AoA=20°, offset=29 mm

Two parameters are used for the characterization of gust; gust ratio and encounter width. The formula (4.1) below is an expression for the gust ratio with V as magnitude of flow disturbance and U_∞ as free stream velocity.

$$GR = \frac{V}{U_\infty} \tag{4.1}$$

The second parameter, encounter width, is calculated with the formula given in (4.2) with w as the gust width and c as chord length. The gust width, w, is considered as the distance between peak to peak value of velocity disturbance.

$$W_e = \frac{w}{c} \tag{4.2}$$

Finally, gust ratio and encounter width are calculated as 1.0 and 0.4 respectively at t=8 s which is just before the negative vortex gust interacts with positive leading edge vortex. Although, the shape of the gust distorts as it travels through the flow field, characterization parameters do not vary drastically. According to fitted polynomials at t=8.5 s given in 2nd column of Figure 4.1, the gust ratio slightly diminishes whereas encounter width does not change. Since changes on the gust parameters are expected as a result of interaction between negative vortex gust and positive leading edge vortex, it is more logical to take values found at t=8 s.

4.3 Observations on Force Data

One of the main objectives of this research is to investigate the effects of AoA on wing loading during gust impingement. Figure 4.2 presents ΔC_L and ΔC_D plotted at same offset value with varying AoA for the experiment set. ΔC_L or ΔC_Drepresents the difference in the force coefficent observed in the presence of the gust encounter with respect to the values obtained in the absence of the gust, in free stream flow.

The general trend of lift coefficient variation shows similarity for the majority of cases. At first, forces acting on the wing are at steady state. However a local maximum in lift is observed slightly after t=5 s associated with start of gust generator motion. This local extreme in force is followed by a minimum peak for lift at around t = 8 s. A process for the recovery of forces starts and another local maximum peak is observed.

Finally, lift coefficient converges to the steady state value. Except AoA=45 ° case at offset values of 19 and 29 mm, general trend mentioned applies to all cases.

Likewise, drag coefficient variation also shows self-similarity for the test cases. Before the start of the gust generator motion, plots fluctuate around steady state values. When the motion starts at t=5 s, a minimum local peak followed by a maximum is observed. It should be noted that timing of these peaks exactly matches timing of peaks of ΔC_L plots, but their sign is opposite. Then, forces start to recover and another local minimum peak is observed. Finally, forces fluctuate around the values observed before the motion of the gust generator and reach steady state.

An observation of Figure 4.2's first row shows that cases become more affected in terms of ΔC_L as AoA gets higher. However, the cases that are least affected by the gust in terms of ΔC_D have high angle of attack values.The local extremes and peak values are considerably smaller compared to cases with low AoA. However, AoA=30° case loses this advantage when offset gets higher. An increase in the recovery time is observed as AoA gets higher. The order of increase in the recovery time is broken by the AoA=30° case.

Another objective of this research is to investigate the effects of offset between the chord of the gust generator and the leading edge of the model on wing loading during gust impingement. Figure 4.3 and Figure 4.4 incluede ΔC_L and ΔC_D data respectively for the same AoA cases with varying offset.

According to Figure 4.3, the extreme peak value of lift coefficient variation gets slightly lower as offset increases. This decrease becomes more prominent at cases with high AoA. However, local extremes are considerably affected by offset difference. The first local maximum around t = 5 s loses its severity whereas the local maximum during the recovery of forces becomes more prominent. Self similarity is observed for all cases except the AoA=45° case.

.Figure 4.4 shows that the extreme peak value of drag coefficient variation gets slightly higher as offset increases. This increase becomes more prominent at cases with high AoA as observed for lift. Likewise, local extremes are considerably affected by offset increase. The first local minimum around t = 5 s loses its severity whereas the local maximum during the recovery of forces becomes more prominent as offset gets higher. All graphs except theAoA=45° case shows self similarity.

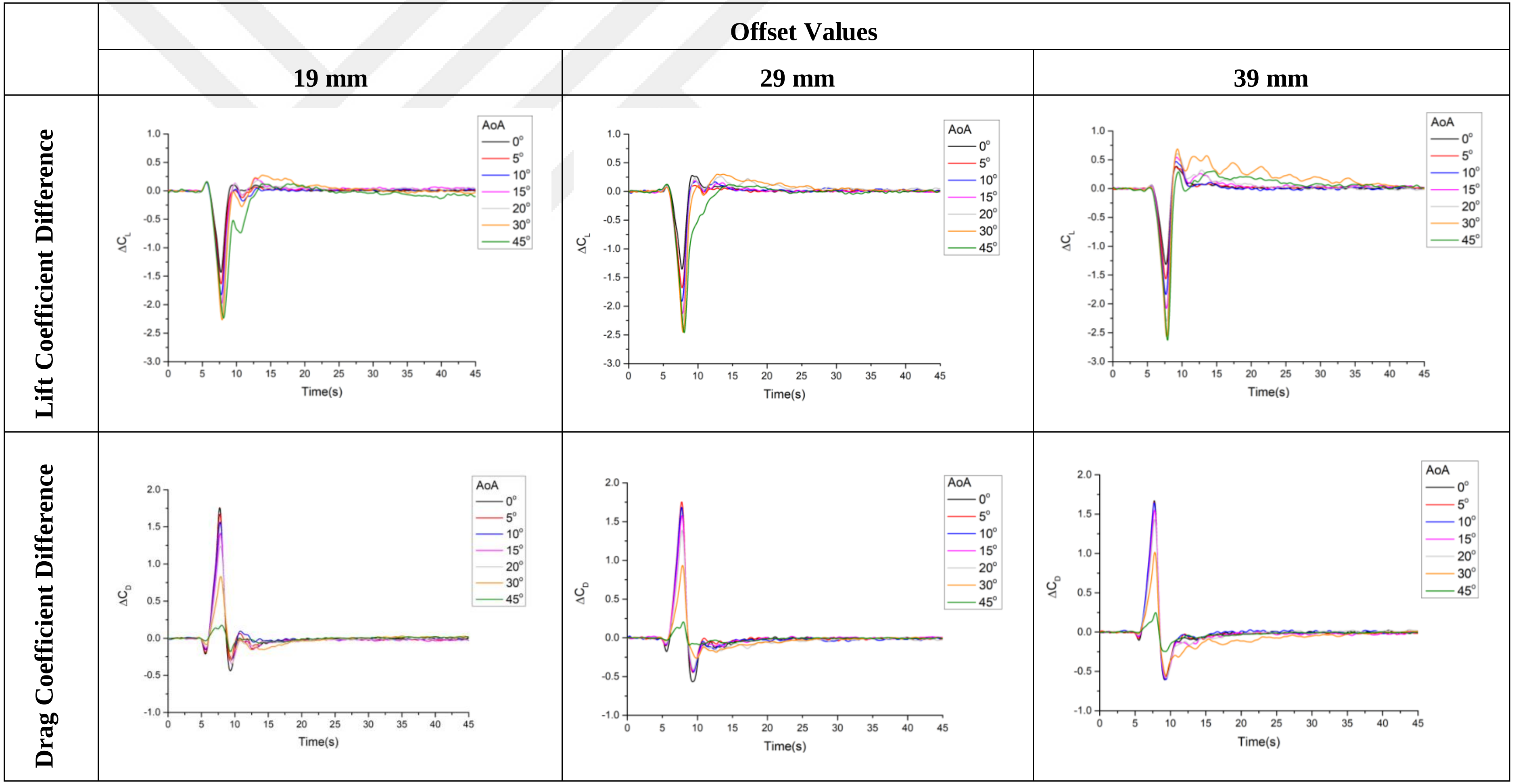

Figure 4.2 A comparison of aerodynamic forces for test cases

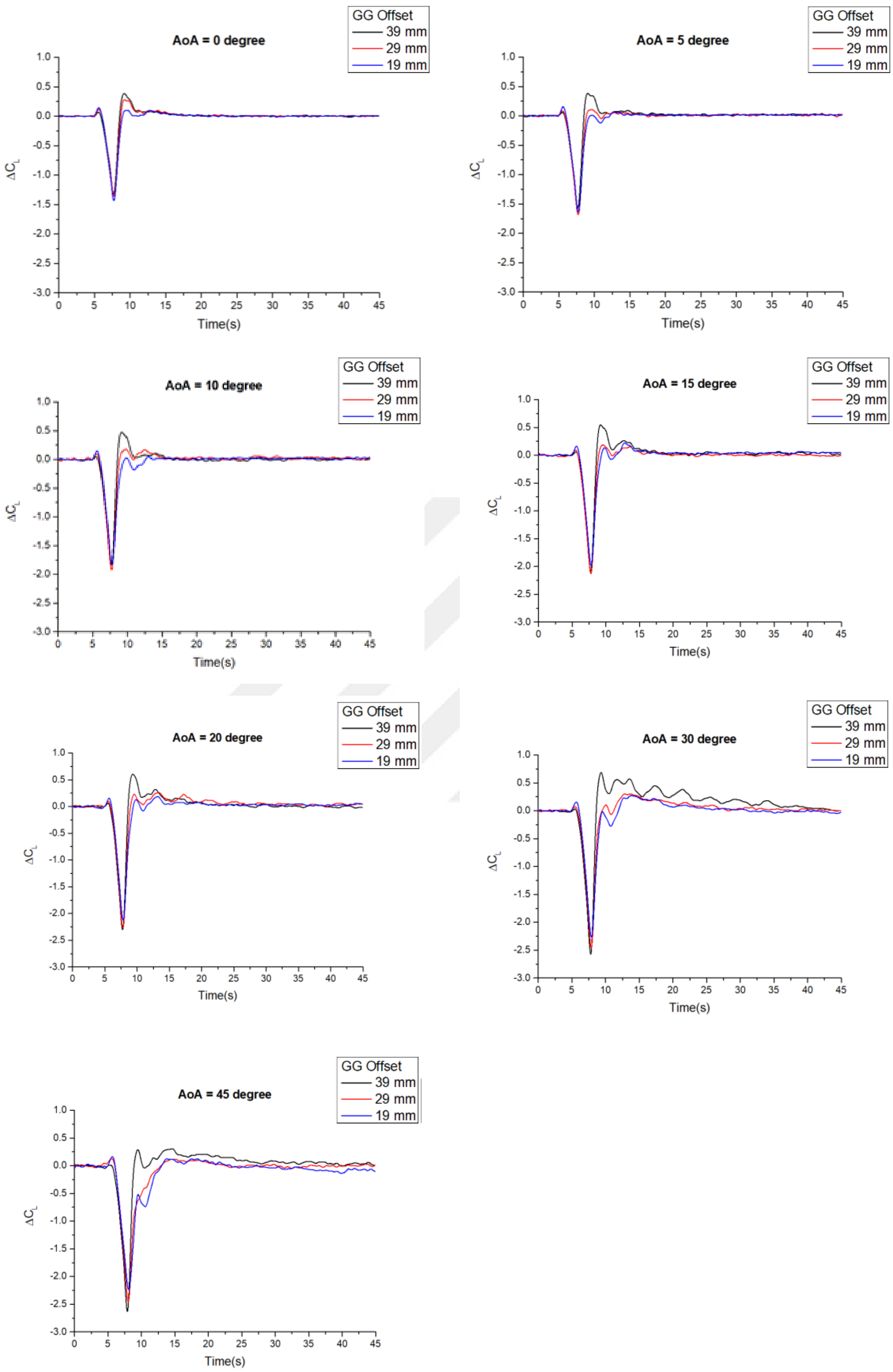

Figure 4.3 Comparison of cases with same AoA in terms of ΔC_L

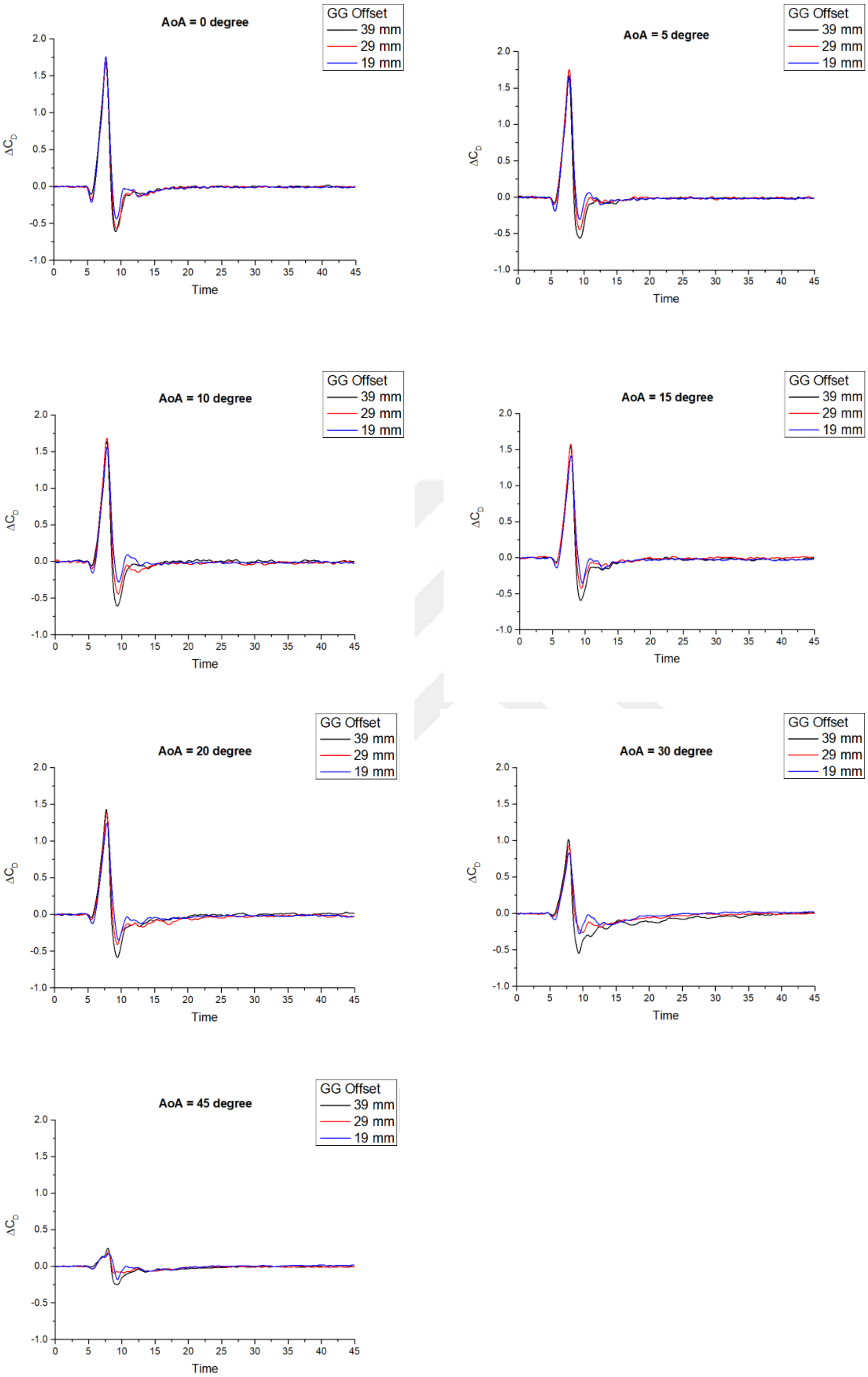

Figure 4.4 Comparison of cases with same AoA in terms of ΔC_D

4.4 Effects on Flow Structures

A moderate angle of attack, AoA=20°, is chosen to study the flow structures during gust impingement. In Figure 4.5, first row of images represents the steady state before gust generator motion begins. There are only minimal fluctuations in force in this time interval and investigation area is devoid of any major vortical structures. The motion starts as the first image of second row is taken. Gust generator creates several small positive vortices during its motion and a strong negative vortex enters the flow field at t=6.5 s. As negative vortex continues its path, a vortex in opposite direction begins to form on the leading edge of model as a reaction to it. At this point both lift and drag coefficient reach their minimum and maximum peaks respectively. At the 3rd row of images, positive leading edge vortex tears itself from model interacting with the negative vortex. As a result, effects of both vortices in flow field are neutralized and forces start to recover at this time interval. The last row shows the flow structures around the model during steady state.

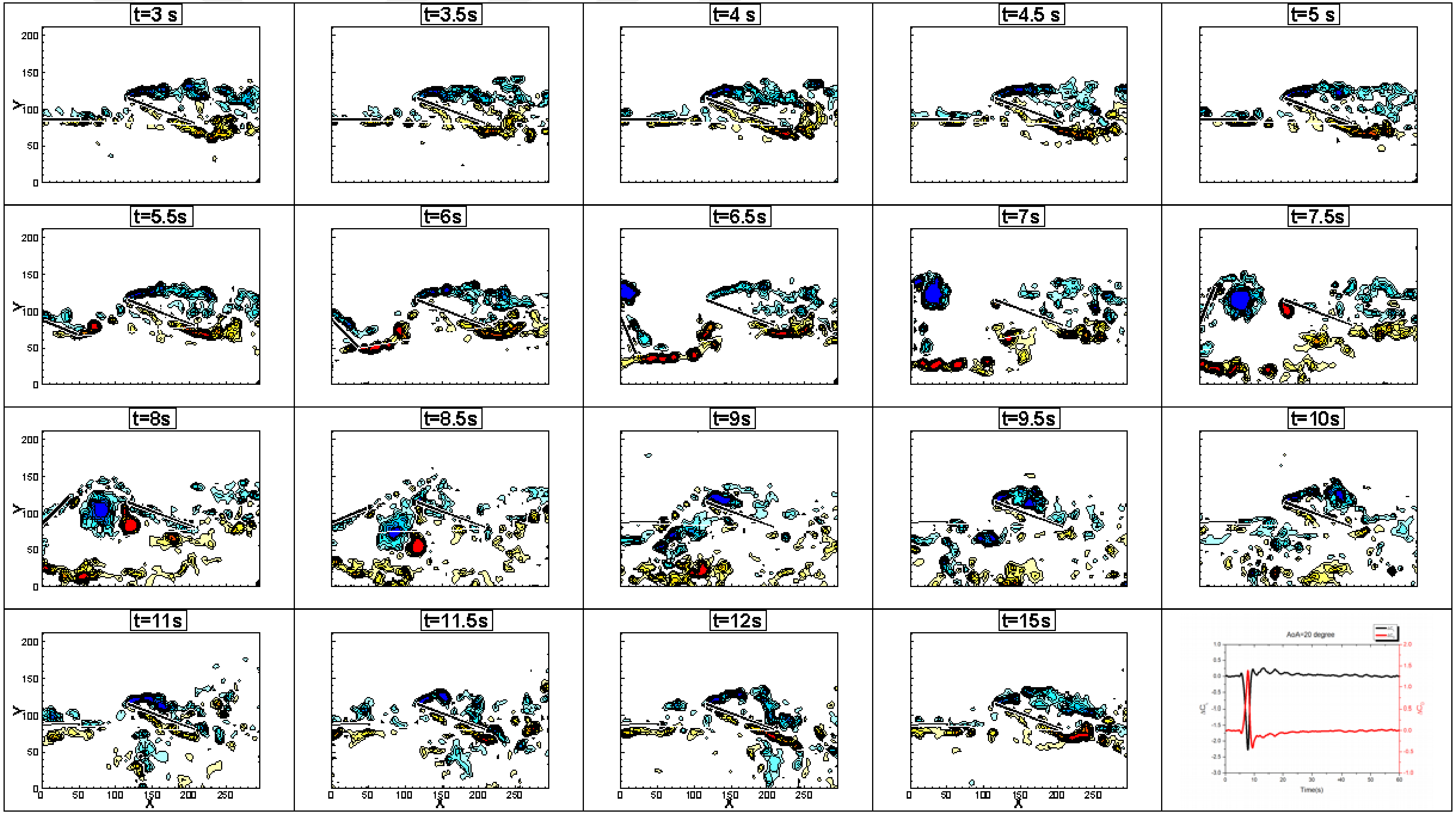

Figure 4.5 DPIV images for Offset=29 mm, AoA=20°

When aerodynamic force variations acting on the model are observed, difference of peak values due to model's AoA is evident. Figure 4.6 shows the DPIV images of at t=8 s which is the time of the extreme peak value for ΔC_L and ΔC_D. Comparing DPIV images at this instance in time shows that as the angle of attack increases for the same y-offsetvalue, the center of the vortex gust shifts to positive y-direction. The positive vortex formed at the leading edge of model becomes weaker as the AoA gets higher and offset gets lower, which might be the cause of substantial decrease in drag coefficient extreme values for cases with high AoA.

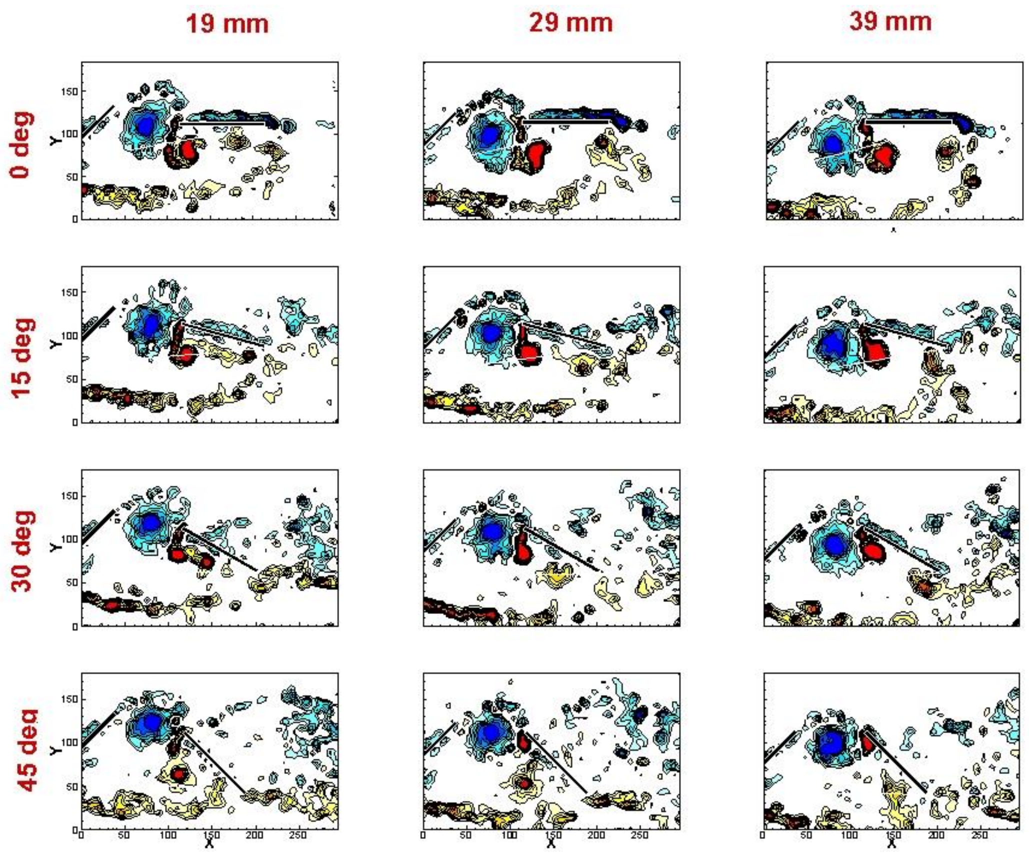

Figure 4.6 DPIV images for t = 8 s for various cases

A comparison for flow structures is done for AoA = 0 and 45°and for y-offset=19 mm and 39 mm in order to understand the effects of these parameters to the process of vortex encounter. Figure 4.7 shows DPIV images from t = 6.5 s to t = 9 s for specified cases.

Flow structures around the wing are affected by small vortices formed at the start of the gust generator motion for offset=19 mm cases. These vortices follow a path towards the wing after their release and interact with positive leading edge vortex as seen at t=7.5 s for 0°case and t=8 s for 45° case. As mentioned before, positive leading edge vortices are weaker at cases with offset=19 mm compared to the ones with offset= 39 mm ones.

Comparison of different AoAs at same offset value shows that the positive leading edge vortex at high AoA is weaker compared to low AoA case. Also a difference in formation instances of leading edge vortex is observed. The positive leading edge vortex is formed at t=7.5 s for AoA=0°, while this formation is delayed to 8 s for AoA=45° case. Generally, gust follows a path towards pressure side of wing while it interacts with leading edge vortex and disperses. However at offset=39 mm case, vortex passes through suction side for AoA=45° case.

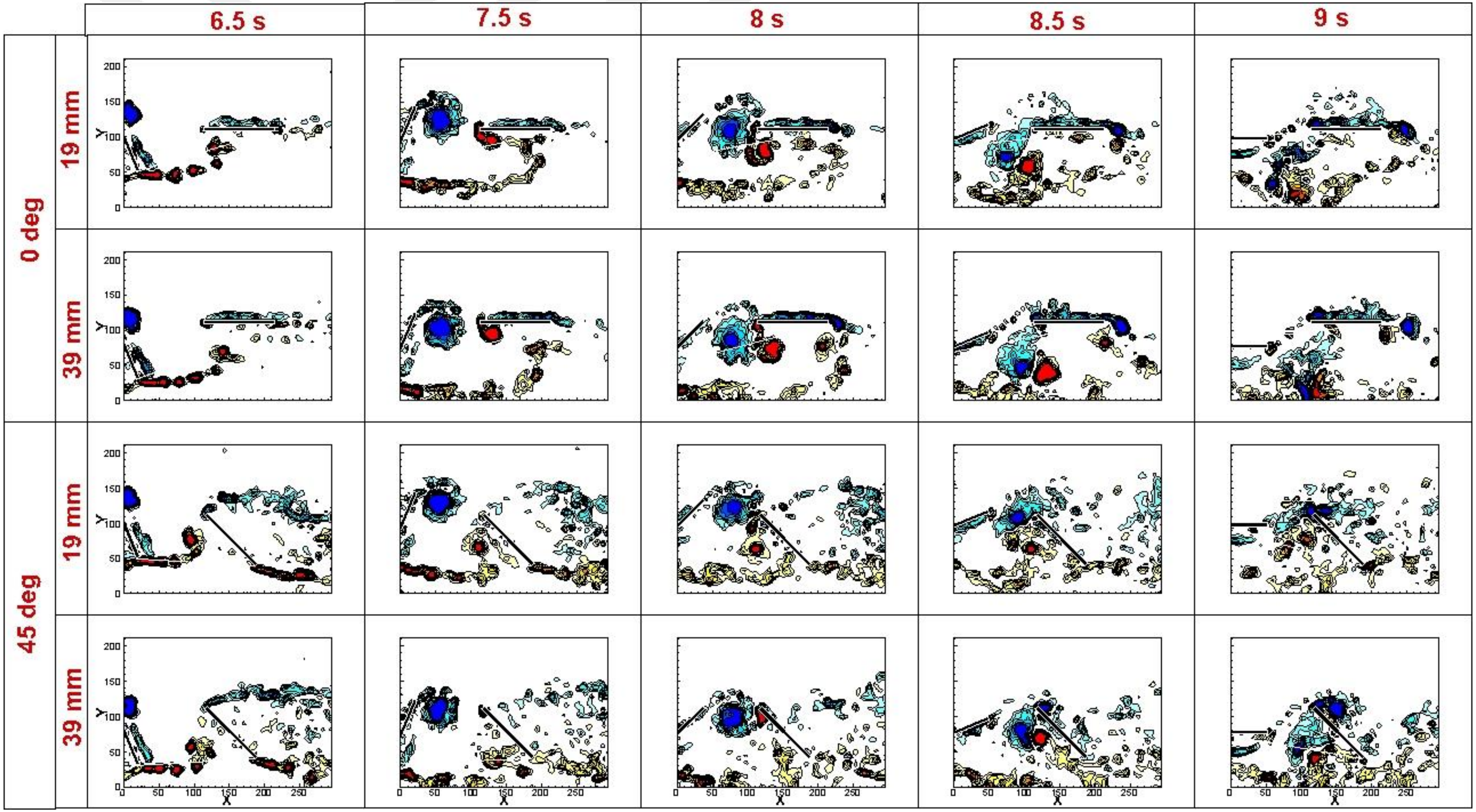

Figure 4.7 Vortex encounter for combinations of AoA = 0° & 45°, y-offset = 19 mm & 39 mm

4.5 Effective Angle of Attack Calculations

An investigation is made to observe a relationship between aerodynamic forces and effective angle of attack during vortex encounter. A chord length vertical line with its center located at 0.25c upstream of the model leading edge is selected as shown in Figure 4.8. Then, u and v velocity values on the line are extracted from DPIV data; velocity values are averaged on the line and effective angle of attack values are calculated with the formula given below;

$$\alpha_{eff} = \alpha + \tan^{-1}\frac{v}{u} \tag{4.3}$$

Since the calculations express effective angle of attack values before flow reaches to the model, results are shifted 0.25 s in time to make an accurate comparison with aerodynamic coefficient variations.

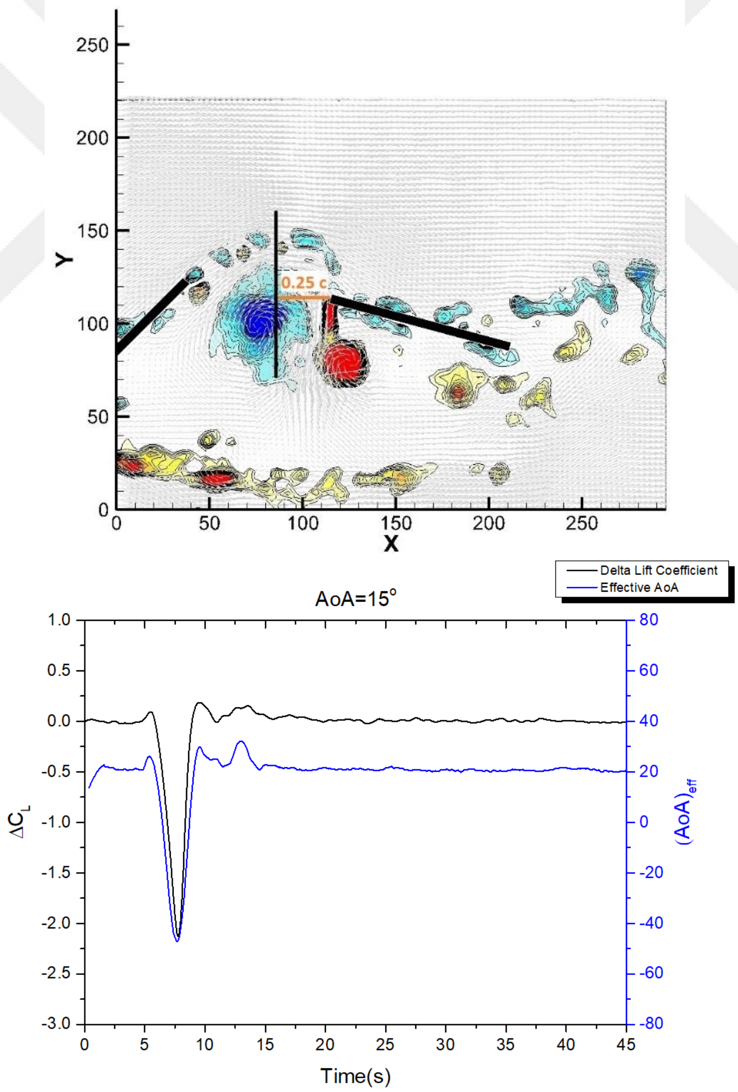

Figure 4.8 : Chosen extraction line and resultant AoA_{eff} comparison with ΔC_L

First, ΔC_L and AoA_{eff} plots of all cases are obtained together to have a clear sight of trends. Majority of plots showed similarities, so a case with a moderate angle of attack such as AoA=15° and an offset such as y-offset=275 mm is chosen to make a generic explanation. Figure 4.8 shows that maximum, minimum and local peaks occur at the same instants for both variations. However, steepness of peaks may differ.

After observing time matching property and similarity of trends for ΔC_L and AoA_{eff} for each cases, an overall comparison is done. Figure 4.9 includes lift coefficient variations on the left and effective angle of attack difference with respect to static value on the right plotted at same offset for varying AoA of the model. The order of magnitudes at the minimum peak is the same for both, cases become more affected as AoA gets higher. However, the difference between peak values of cases is more distinctive on the left side of the figure. On the right side, only the AoA=45°case has a clear diversion from other cases when it comes to the peak value. The trend of ΔAoA_{eff} catches the trend of ΔC_L for first local maximum and minimum peaks. However, its similarity starts to detoriate after recovery from minimum peak for cases with high angle of attack. The similarity is again maintained after recovery for cases with low AoA.

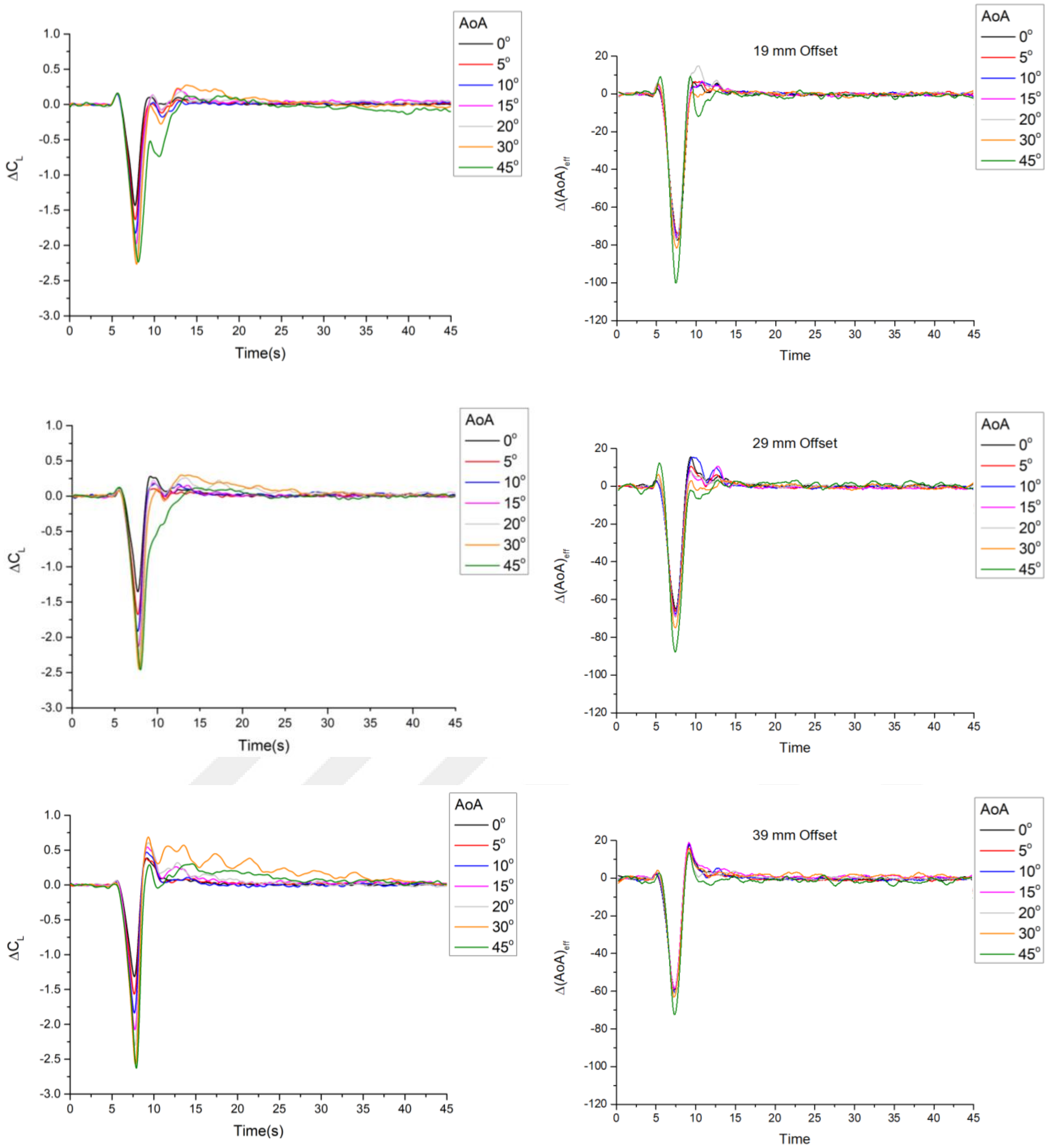

Figure 4.9 : Comparison of ΔC_L and ΔAoA_{eff}

Since a detoriation of similarity is observed for ΔC_L and ΔAoA_{eff} trends at high angle of attack values, the extraction line is stretched and new results for effective angle of attack values are investigated for AoA = 0° and 45° cases.

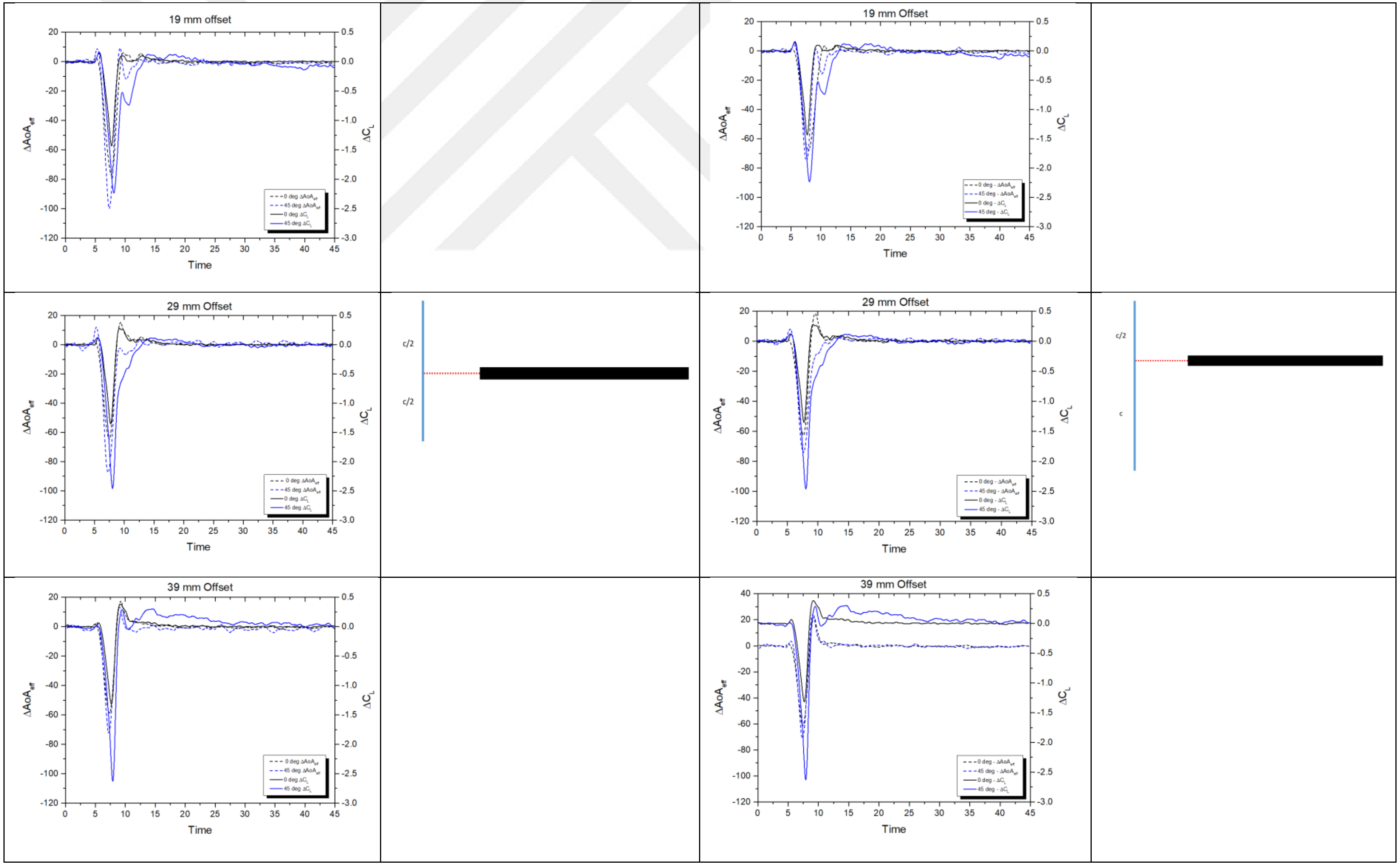

Figure 4.10 Comparison of two extraction lines in terms of ΔC_L and ΔAoA_{eff} for AoA = 0° and 45°

Chosen extraction lines are shown in Figure 4.10 with ΔC_L and resultant ΔAoA_{eff} plots on their left side. The plots given for stretched extraction line are able to catch ΔC_L trend better for AoA=45° cases compared to previous graphs. Particularly, recovery after extreme peak at offset=29 mm is well captured. However, ΔC_L's second local peak shown in the last row is still not observed in the newly calculated ΔAoA_{eff}. A comparison with previous calculations of ΔAoA_{eff} for AoA = 0° cases show that current calculations are also reliable for low angle of attack values. In light of this information, stretched extraction line is a better choice in the calculation of ΔAoA_{eff}.

6. CONCLUSIONS AND RECOMMENDATIONS

In this study, effects of single spanwise vortex impingement on flow structures and wing loading is experimentally investigated. 7 angle of attack values and 3 vertical offset of gust generator with respect to model leading edge are combined and investigated to have a better understanding of phenomena. Flow structures in the investigation area during singular vortex impingement are captured by a DPIV system while forces acting on the model are acquired simultaneously by a force/torque sensor.

Forces for different AoAs for the same gust generator position and forces for the same AoA at different gust generator positions are compared. Following this procedure, images gathered by theDPIV system are investigated in conjunction with force data. Major findings of this study can be summarized as follows;

- The general trend of aerodynamic forces acting on model due to vortex impingement shows similarity. However, a difference in the local extreme values are observed in force coefficients associated with the AoA of the model. When drag coefficient variation results are compared, it can be seen that higher AoA values enable the model to be less affected by vortex impingement. However, lift becomes more affected as AoA increases.
- The interaction between negative vortex introduced by the gust generator and positive leading edge vortex of model dominates the flow field. This interaction also affects aerodynamic forces acting on the model.
- Self-similarity for flow structures during the gust encounter is also observed. However, increment of AoA or offset affects formation instants or strength of these structures.

A more detailed study when the impinging vortex sign, strength and size are different is necessary for further investigations. Although the strength and the size of the vortex, therefore the gust ratio and width of the encounter can not be independently varied, those characteristic parameters are recommended to be investigated in future studies.

REFERENCES

Barnes, C. J., & Visbal, M. R. (2017). Effects of vertical position and orientation on a vortical-gust/airfoil interaction at a transitional Reynolds number. In 47th AIAA Fluid Dynamics Conference (p. 3320).

Biler, H., Badrya, C., & Jones, A. R. (2019). Experimental and computational investigation of transverse gust encounters. AIAA Journal, 57(11), 4608-4622.

Corkery, S. J., Babinsky, H., & Harvey, J. K. (2018). On the development and early observations from a towing tank-based transverse wing–gust encounter test rig. Experiments in Fluids, 59(9), 135.

Corkery, S. J., Babinsky, H., & Harvey, J. K. (2018). On the development and early observations from a towing tank-based transverse wing–gust encounter test rig. Experiments in Fluids, 59(9), 135.

Fenercioglu, I. (2010). Experimental Investigation of Flow Structures Around an Oscillating Airfoil in Steady Current. Istanbul: Ph.D. Thesis. Istanbul Technical University.

Hahn, D. G., Klein, S., Scholz, P., & Radespiel, R. (2013). Vortex interactions with a high-lift airfoil in a low speed wind tunnel. In 43rd AIAA Fluid Dynamics Conference (p. 2875).

Hufstedler, E., & McKeon, B. J. (2016). Isolated gust generation for the investigation of airfoil-gust interaction. In 46th AIAA Fluid Dynamics Conference (p. 4257).

Hufstedler, E. A., & McKeon, B. J. (2019). Vortical gusts: experimental generation and interaction with wing. AIAA Journal, 57(3), 921-931.

Jones, A. R., & Cetiner, O. (2020). Overview of NATO AVT-282: Unsteady Aerodynamic Response of Rigid Wings in Gust Encounters. In *AIAA Scitech 2020 Forum* (p. 0078).

Medina, A., Babu, A. V., Rockwood, M., Gopalarathnam, A., & Ahmed, A. (2019). Theoretical and experimental study of wake encounters on unsteady airfoils. In AIAA SciTech 2019 Forum (p. 0898).

Moushegian, A., & Smith, M. J. (2019). Analysis of a wing moving through a nonlinear gust. In AIAA SciTech 2019 Forum (p. 0637).

Mulleners, K., Mancini, P., & Jones, A. R. (2017). Flow development on a flat-plate wing subjected to a streamwise acceleration. AIAA Journal, 55(6), 2118-2122.

Watkins, S., Milbank, J., Loxton, B. J., & Melbourne, W. H. (2006). Atmospheric winds and their implications for microair vehicles. AIAA journal, 4 4(11), 2591-2600.

Wei, N. J., Kissing, J., & Tropea, C. (2019). Generation of periodic gusts with a pitching and plunging airfoil. Experiments in Fluids, 60(11), 166.

APPENDICES

APPENDIX A : Vortex Encounter DPIV Images

APPENDIX A : Vortex Encounter DPIV Images

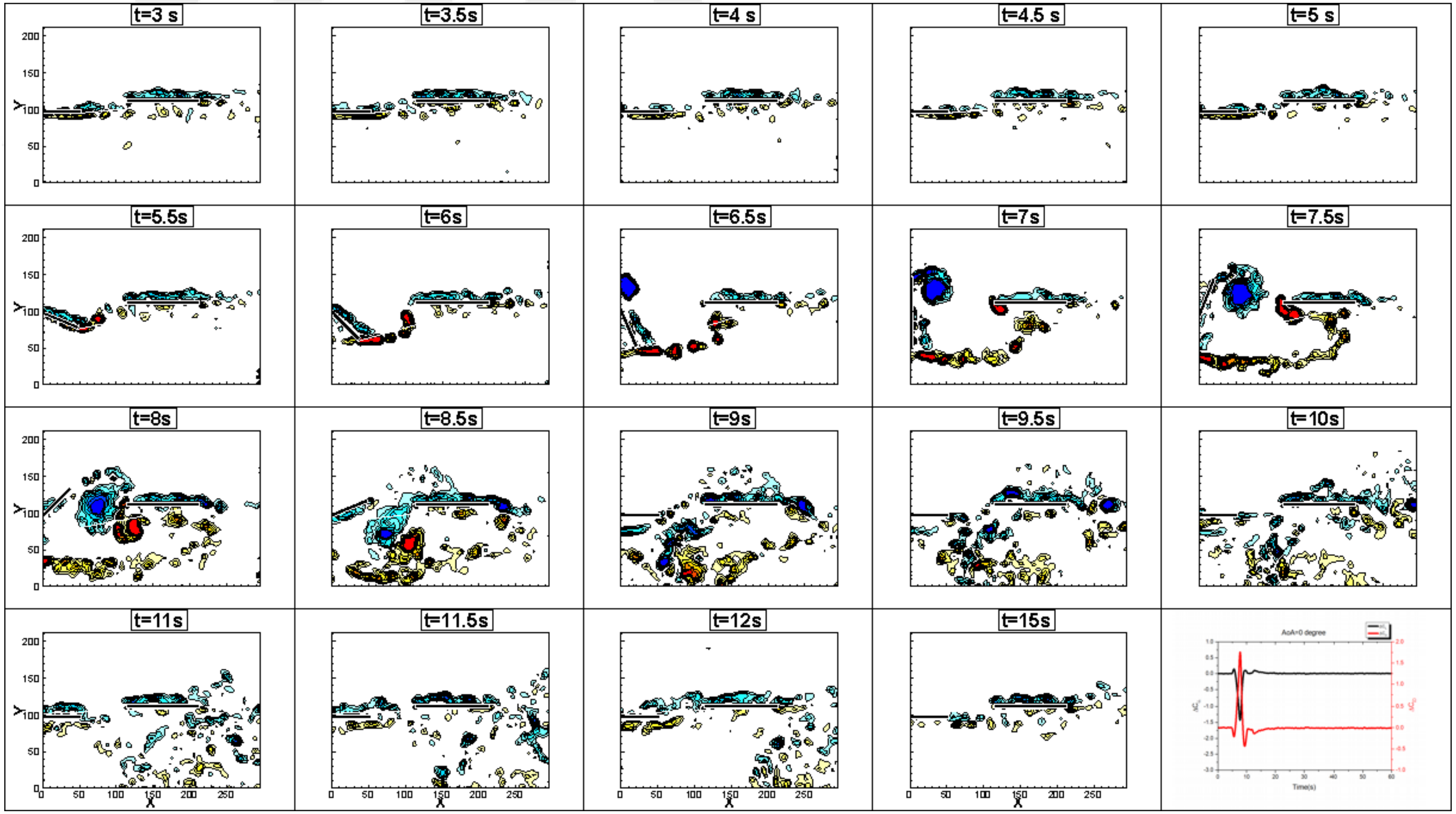

Figure A.1 Vortex Encounter DPIV Images for AoA=0 °, offset=19 mm

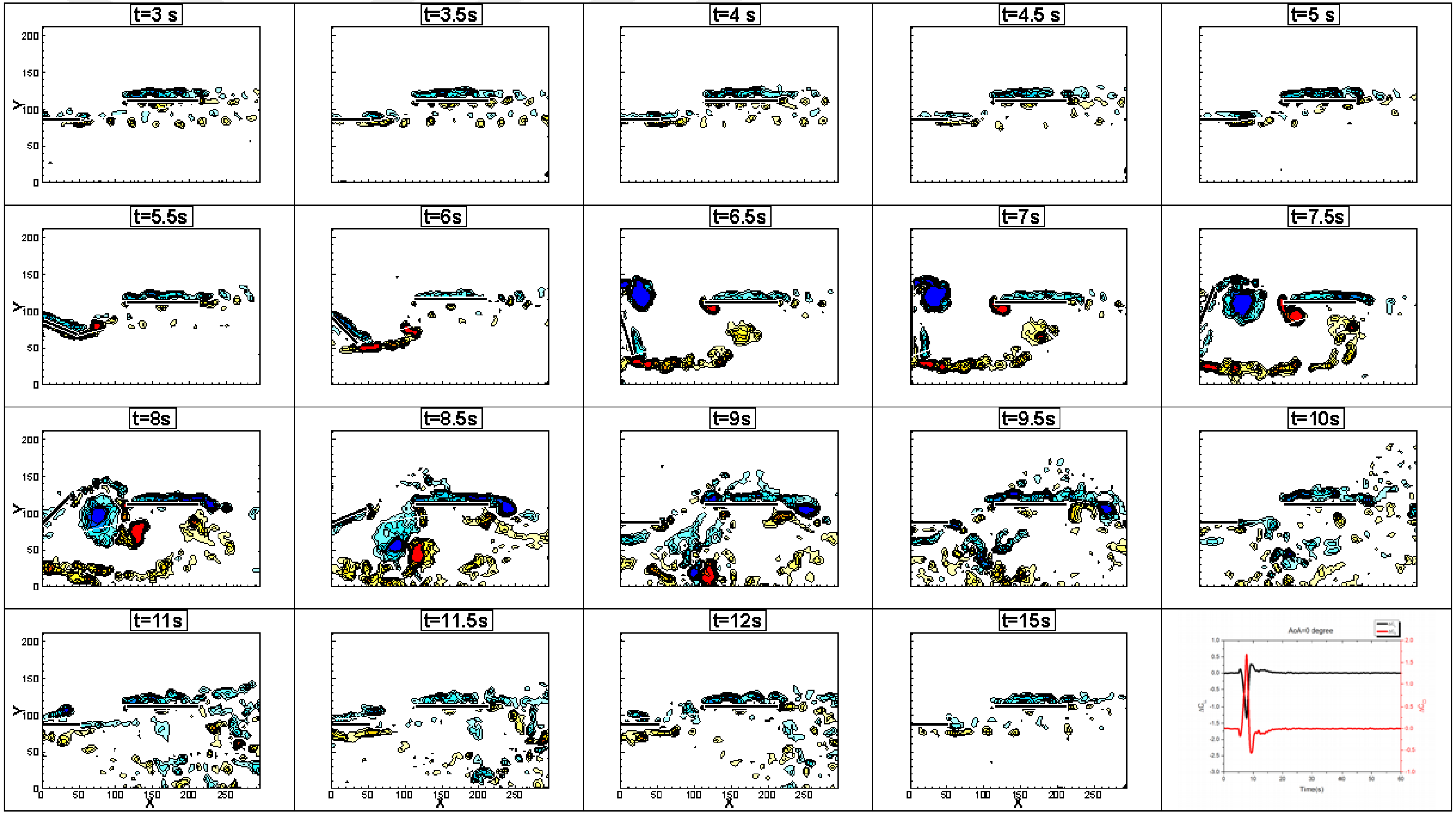

Figure A.2 Vortex Encounter DPIV Images for AoA=0 °, offset=29 mm

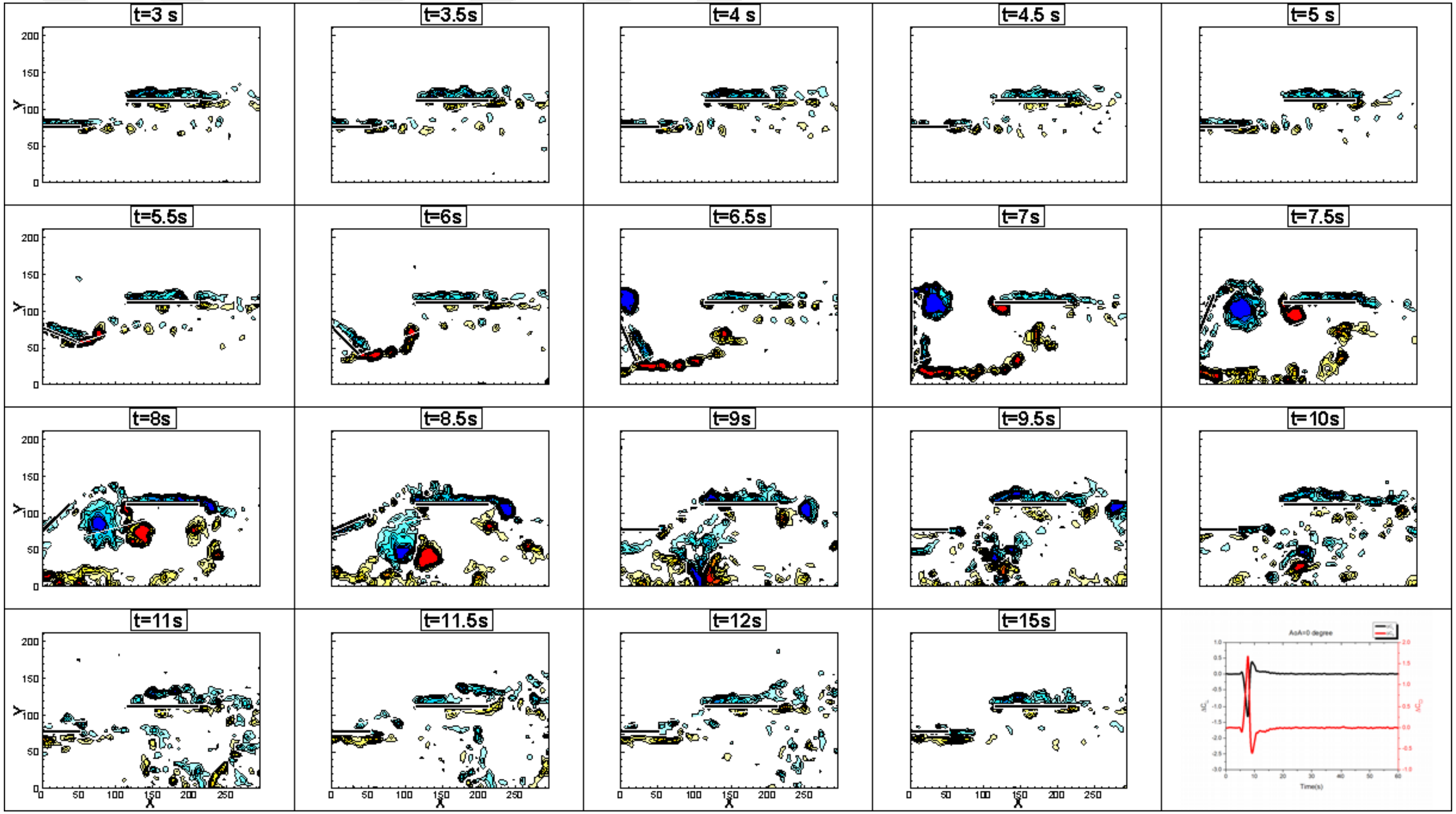

Figure A.3 Vortex Encounter DPIV Images for AoA=0 °, offset=39 mm

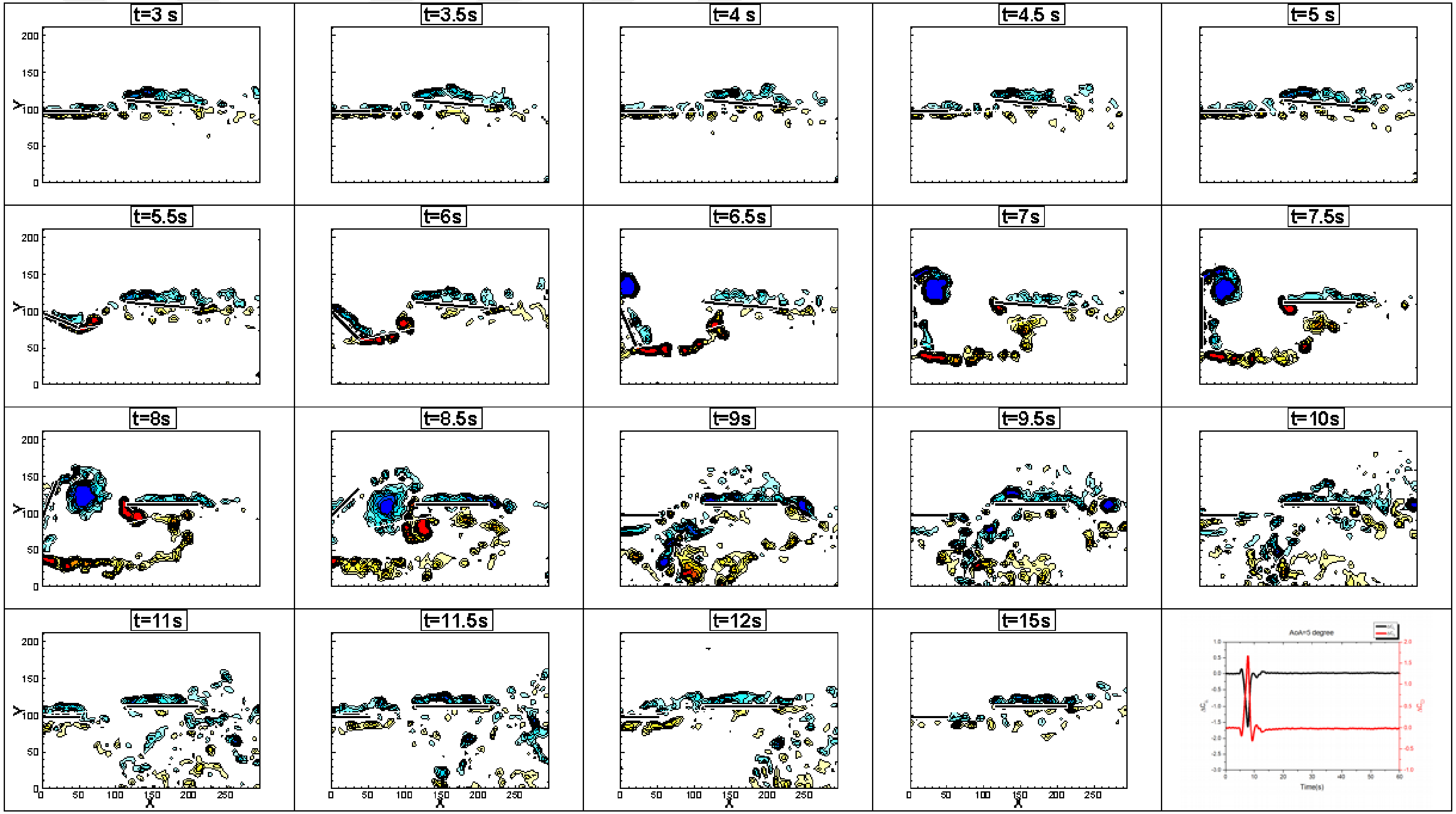

Figure A.4 Vortex Encounter DPIV Images for AoA=5 °, offset=19 mm

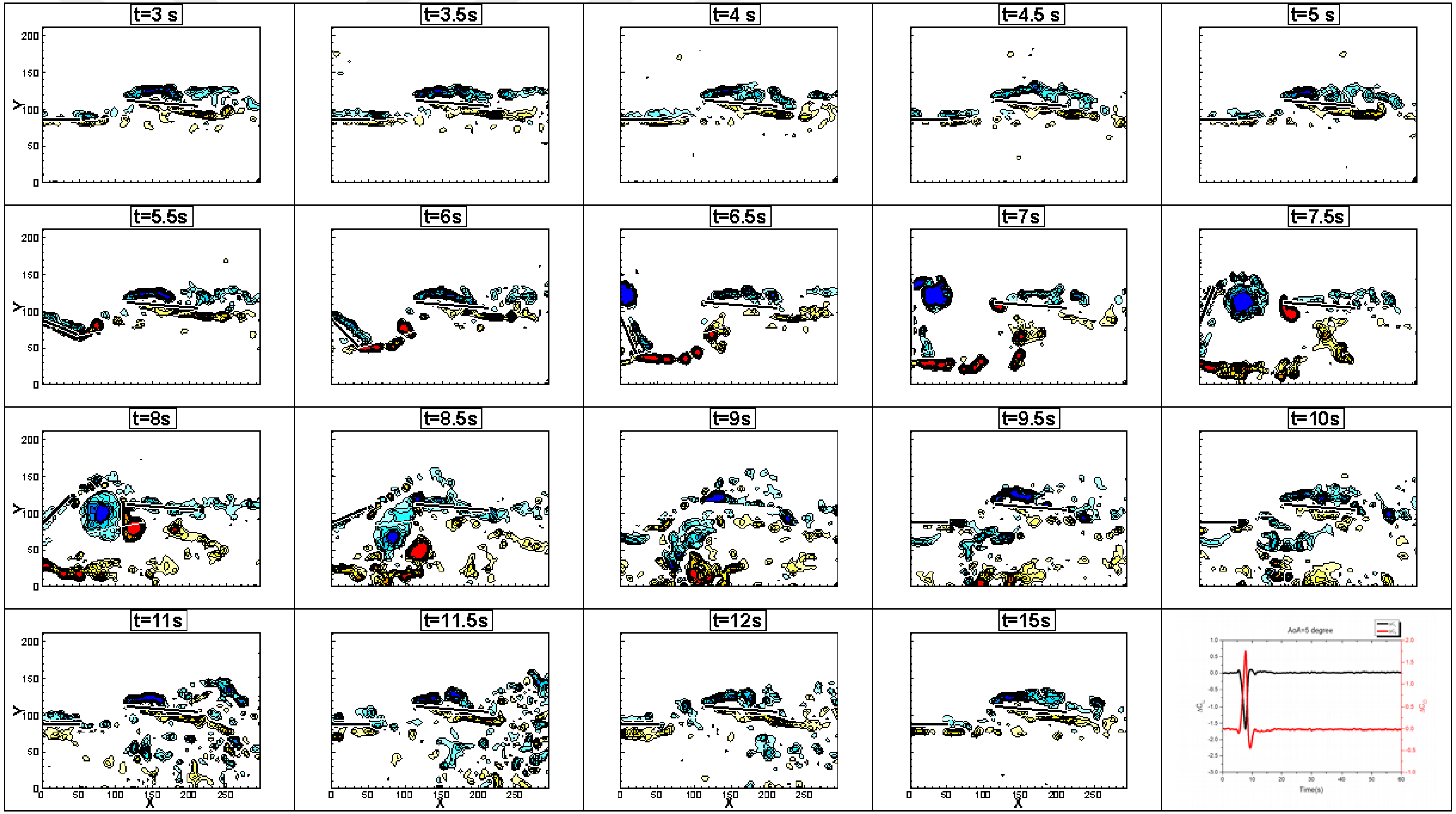

Figure A.5 Vortex Encounter DPIV Images for AoA=5 °, offset=29 mm

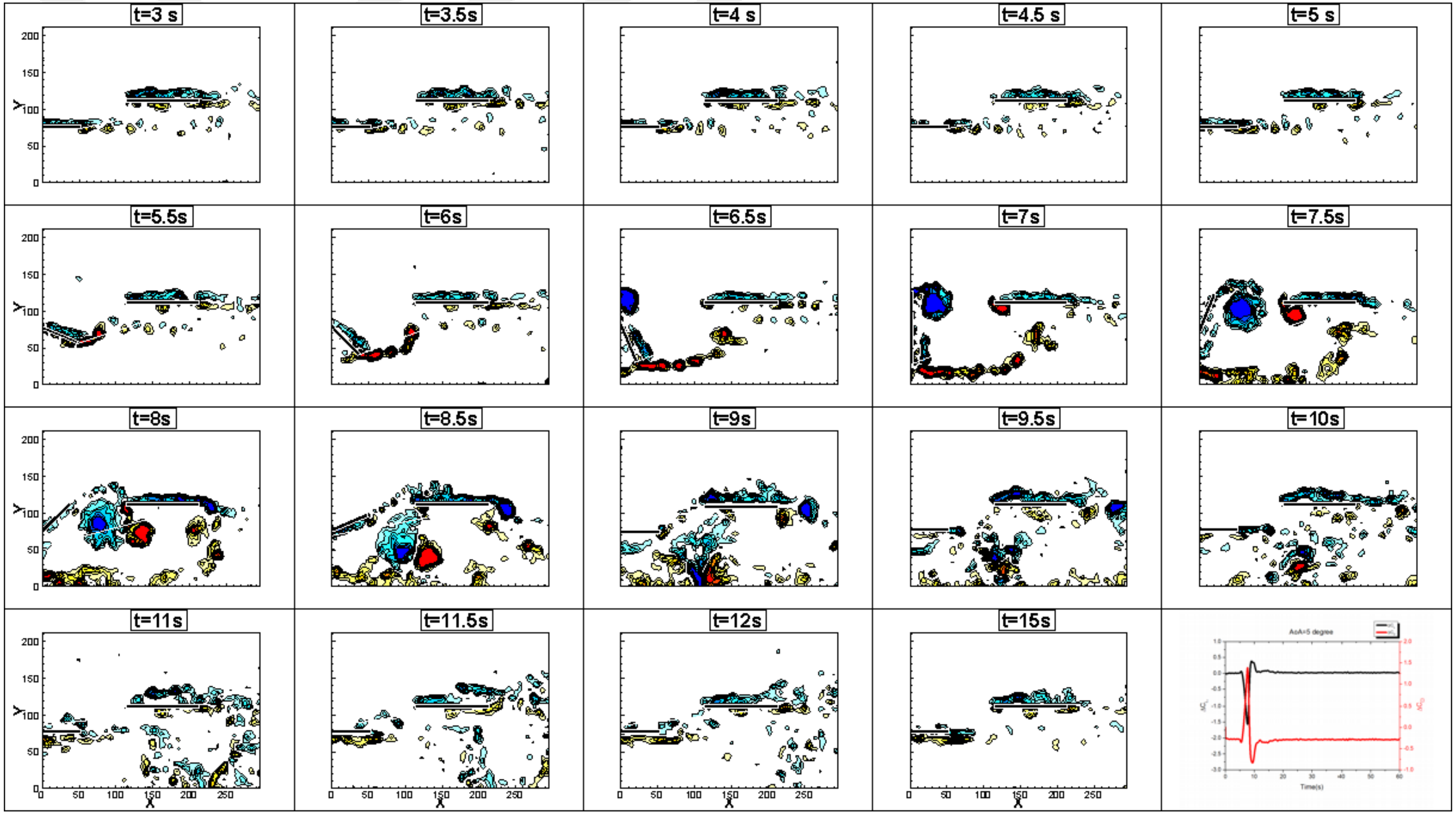

Figure A.6 Vortex Encounter DPIV Images for AoA=5 °, offset=39 mm

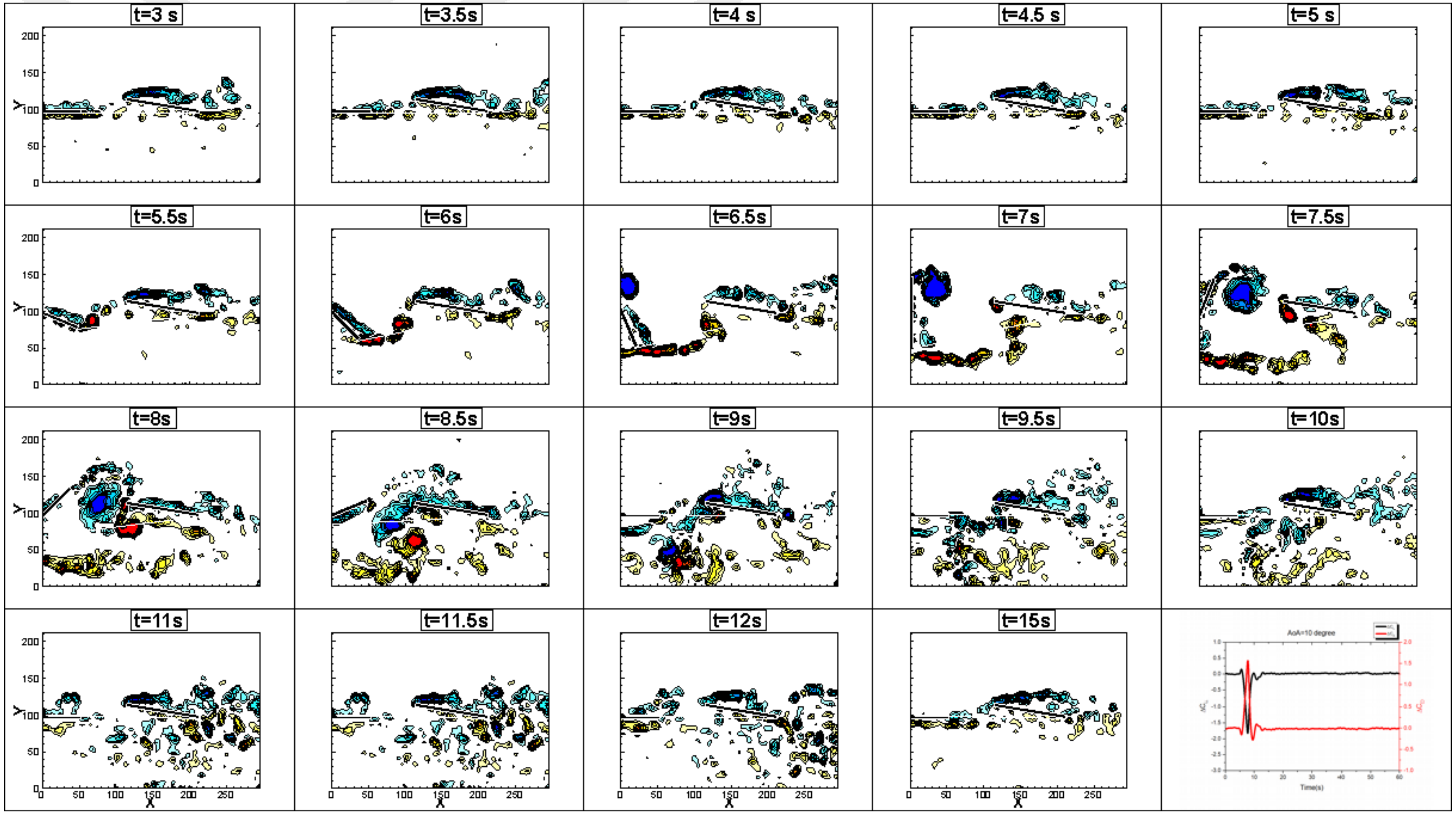

Figure A.7 Vortex Encounter DPIV Images for AoA=10 °, offset=19 mm

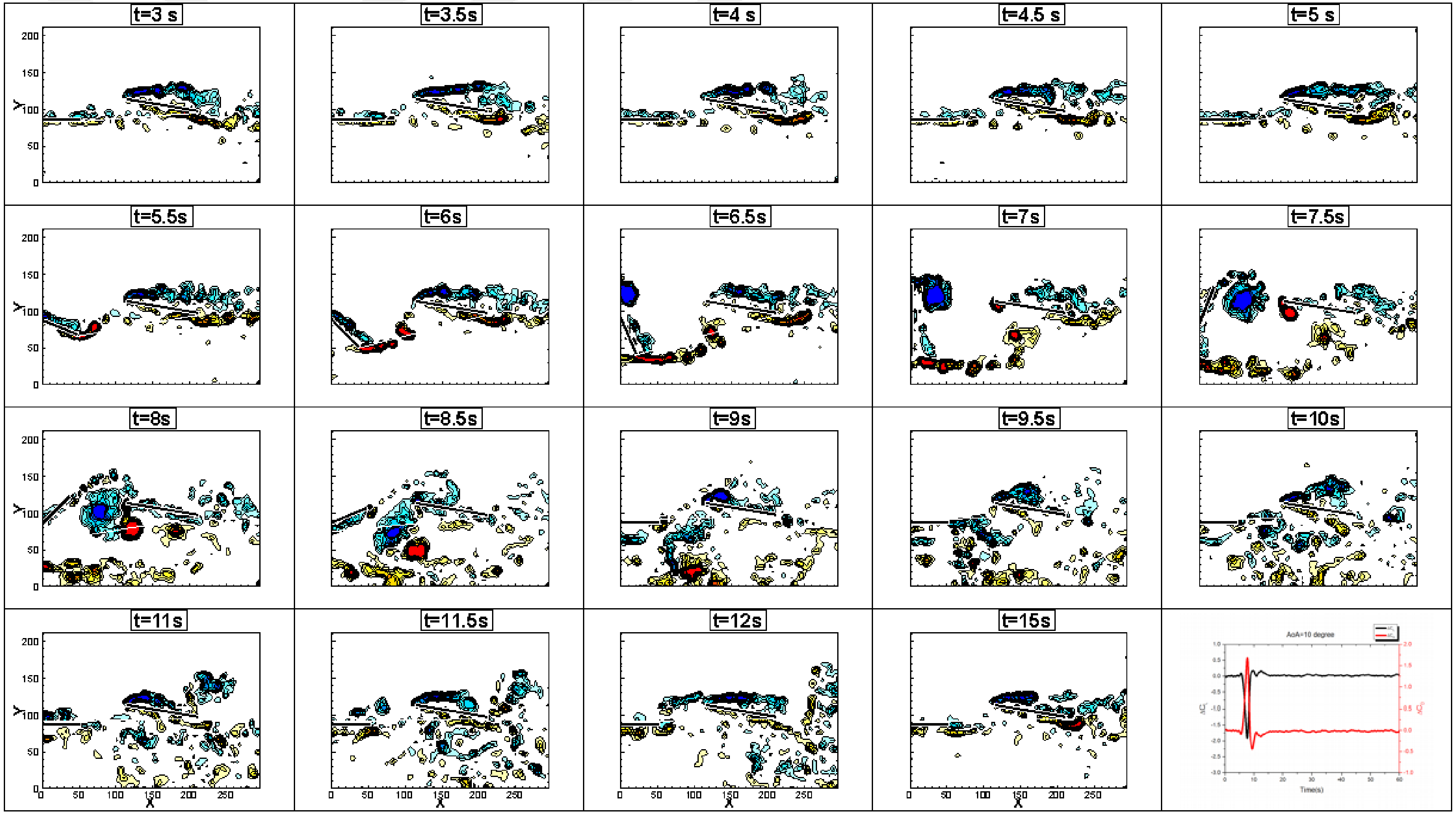

Figure A.8 Vortex Encounter DPIV Images for AoA=10 °, offset=29 mm

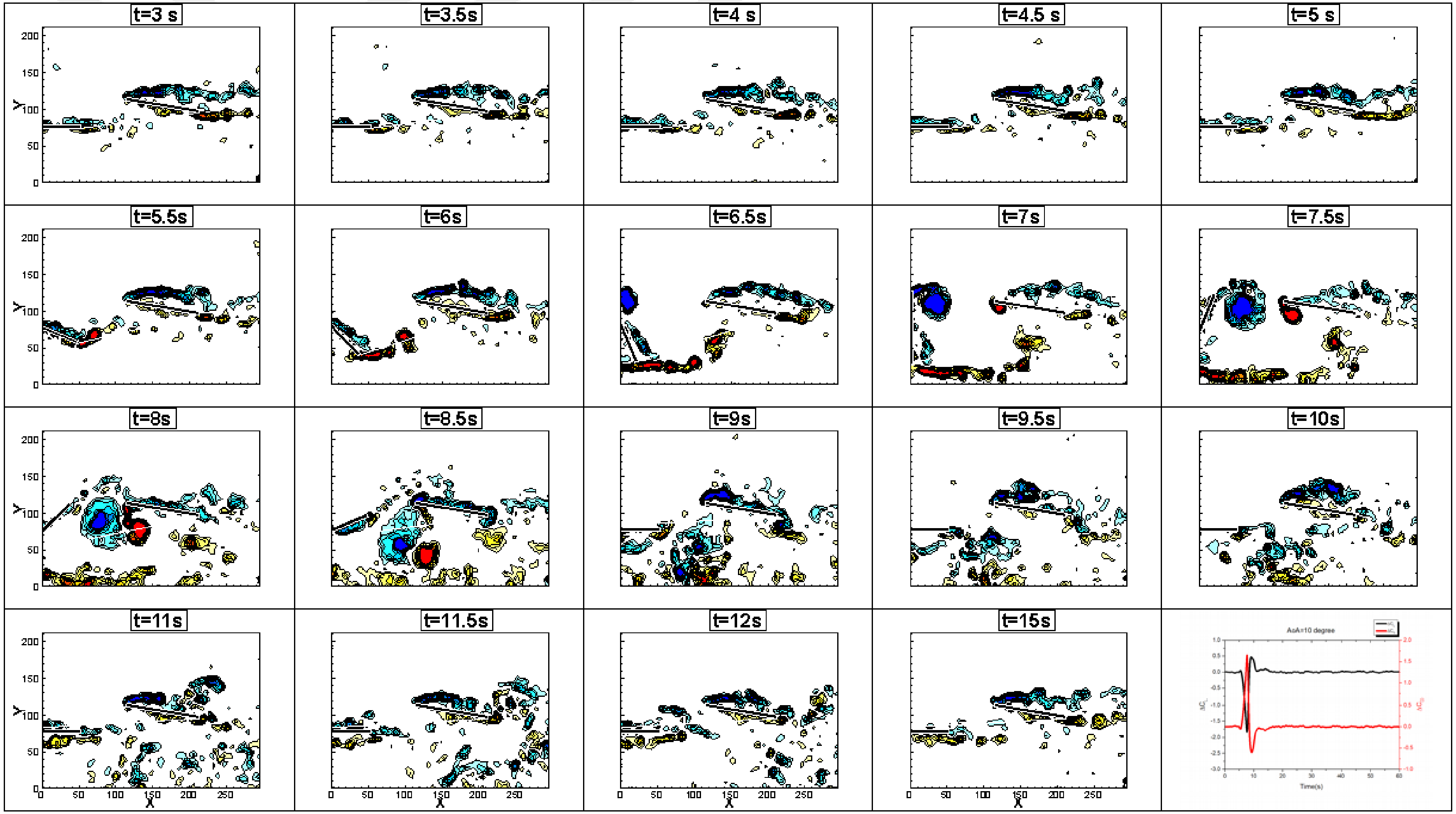

Figure A.9 Vortex Encounter DPIV Images for AoA=10 °, offset=39 mm

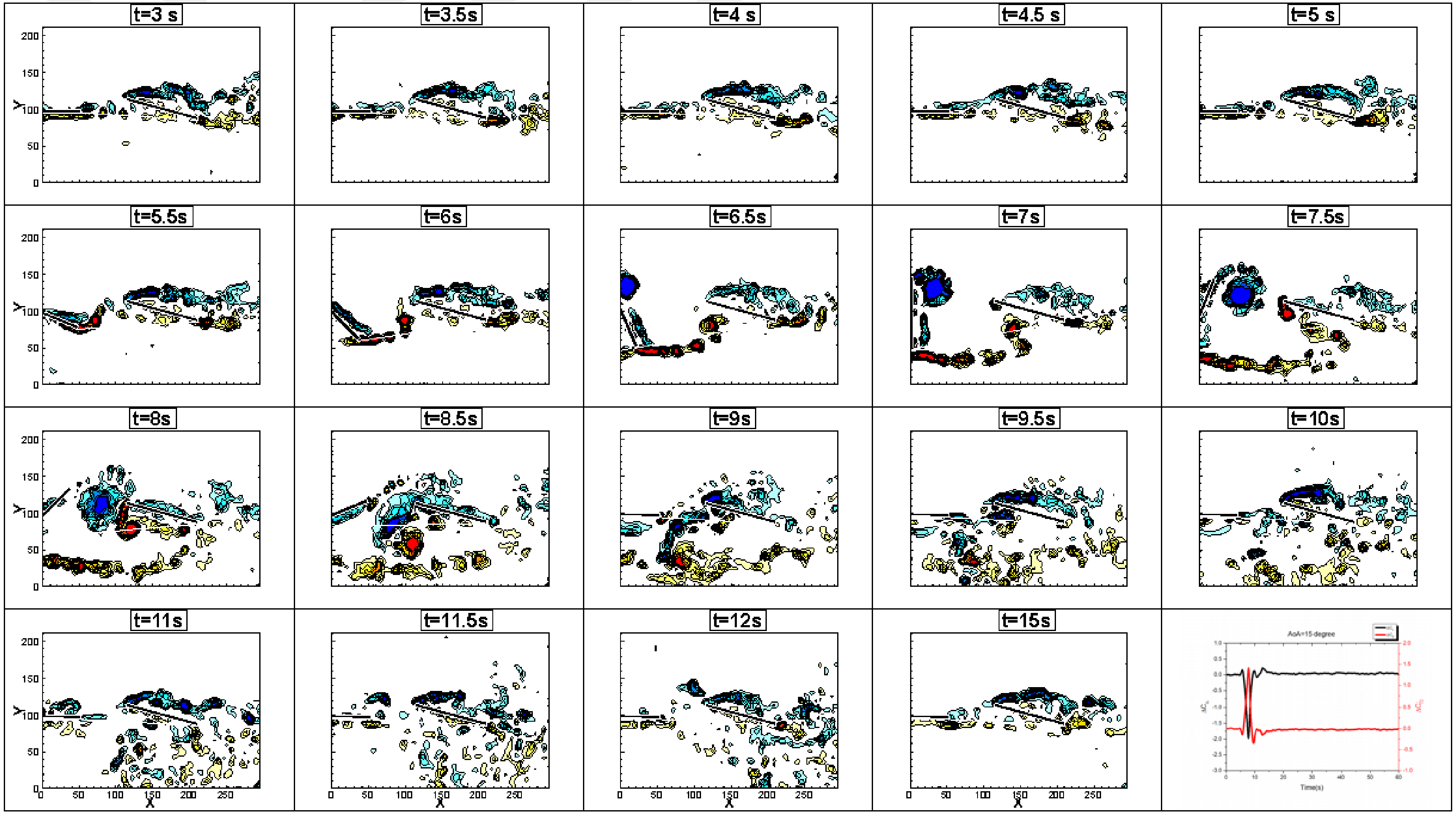

Figure A.10 Vortex Encounter DPIV Images for AoA=15 °, offset=19 mm

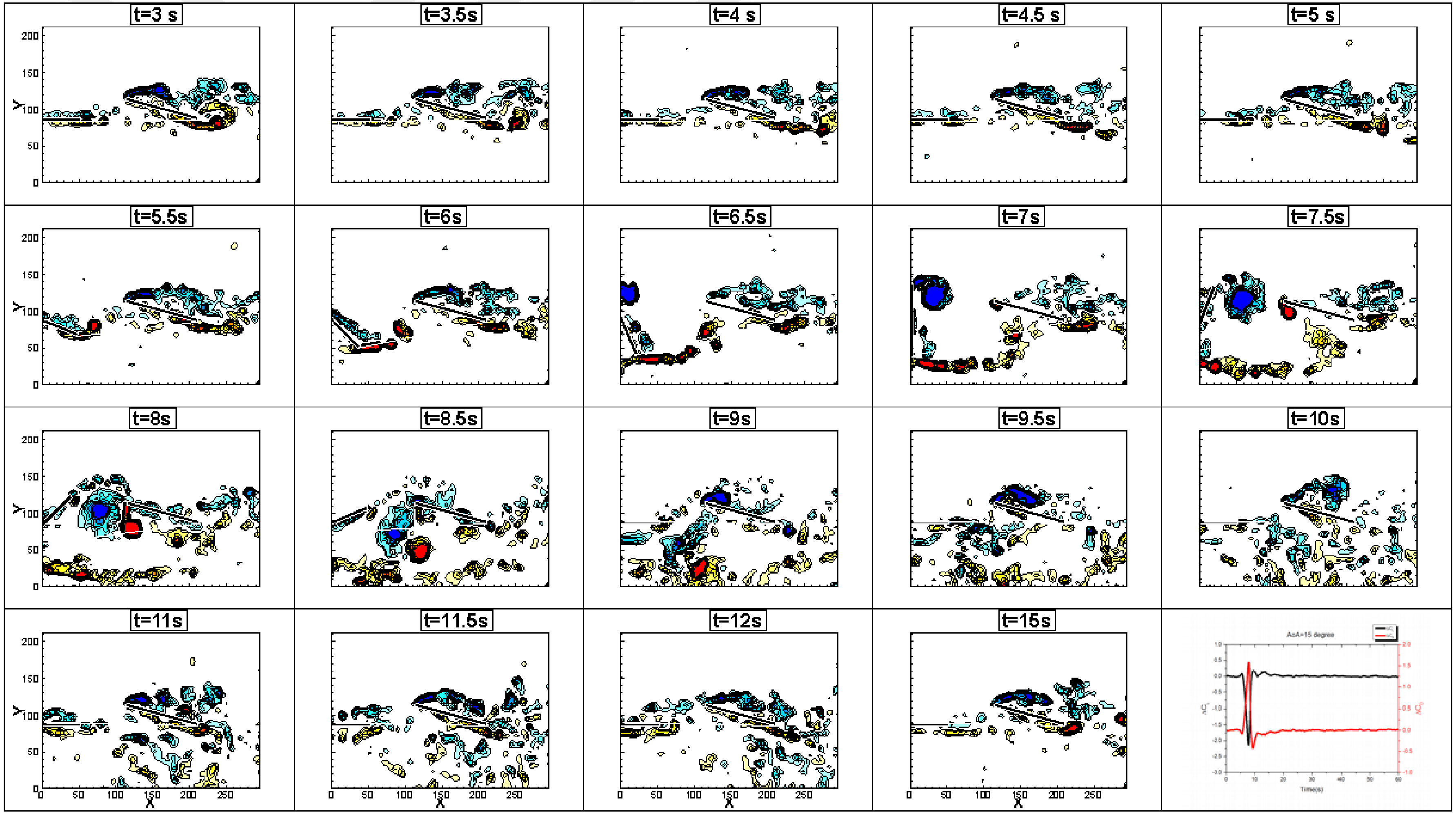

Figure A.11 Vortex Encounter DPIV Images for AoA=15 °, offset=29 mm

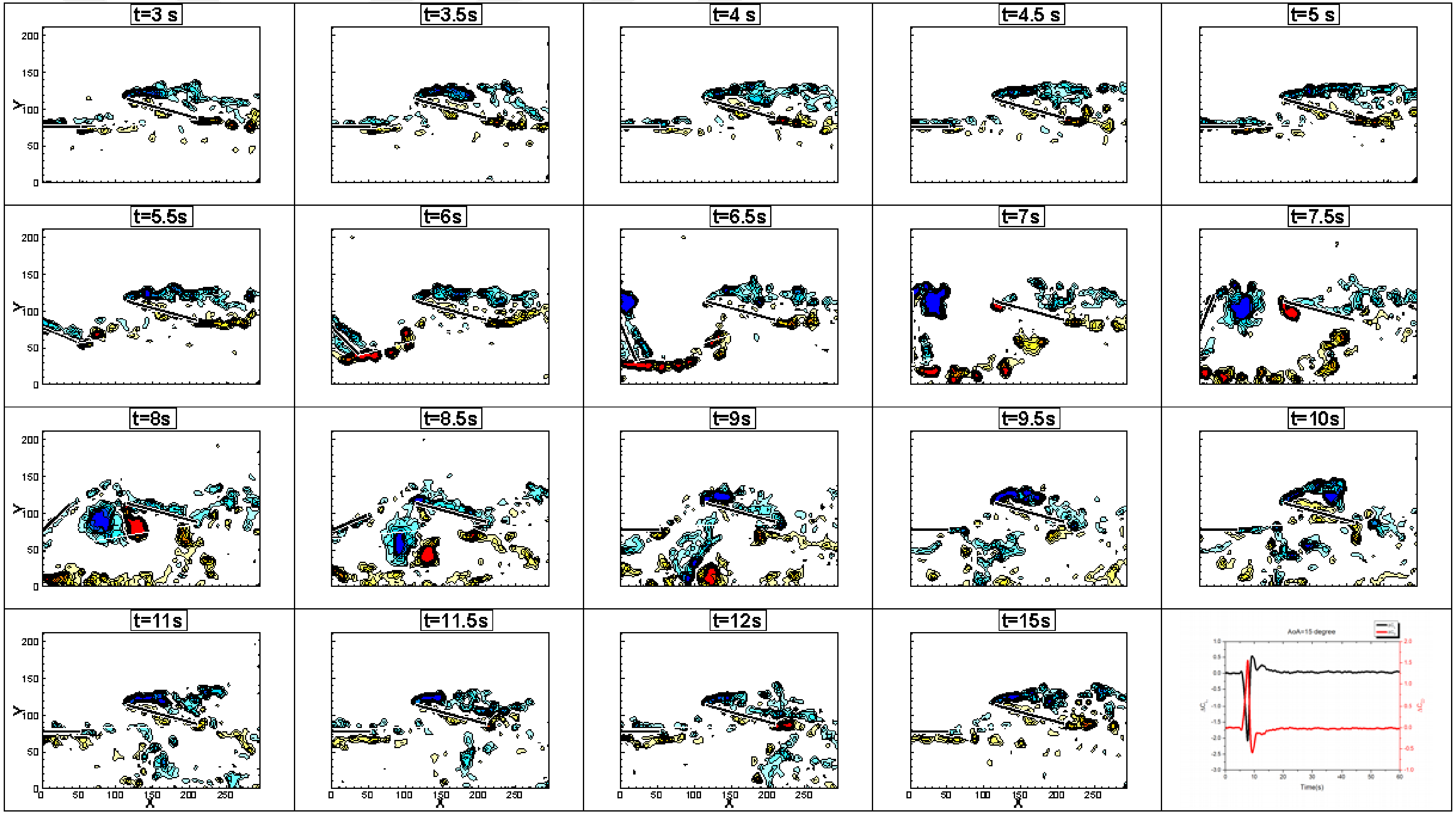

Figure A.12 Vortex Encounter DPIV Images for AoA=15 °, offset=39 mm

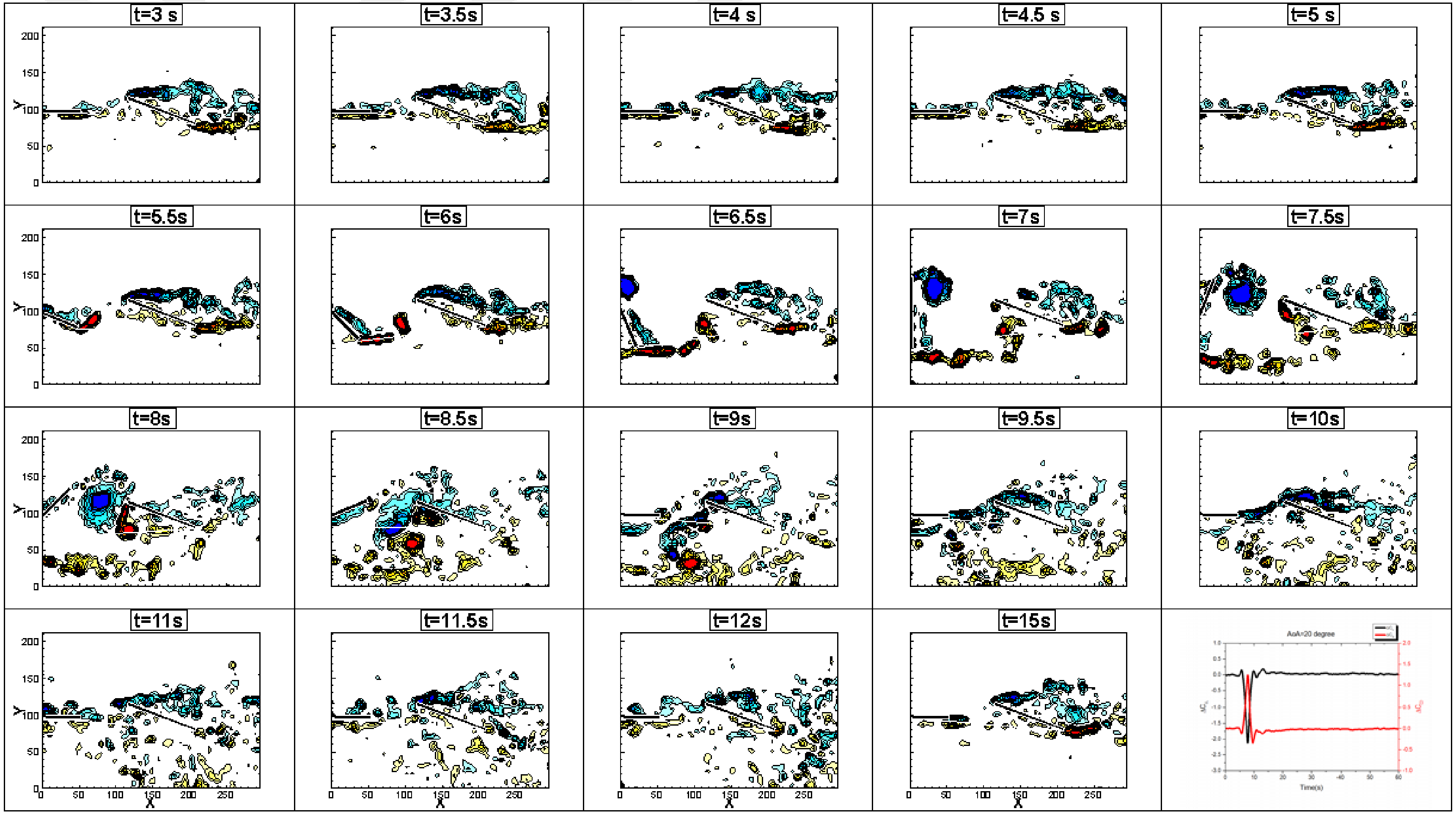

Figure A.13 Vortex Encounter DPIV Images for AoA=20 °, offset=19 mm

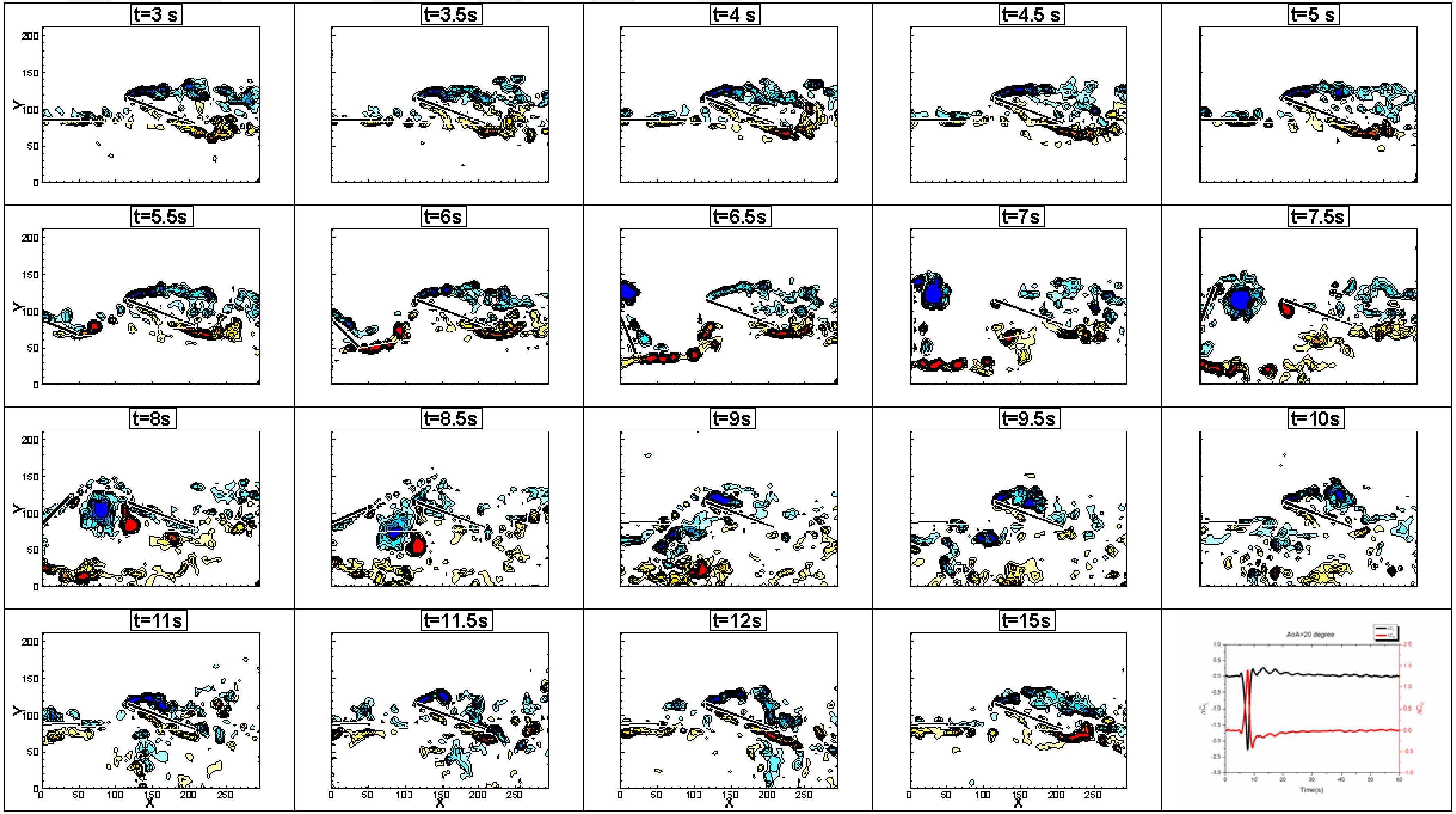

Figure A.14 Vortex Encounter DPIV Images for AoA=20 °, offset=29 mm

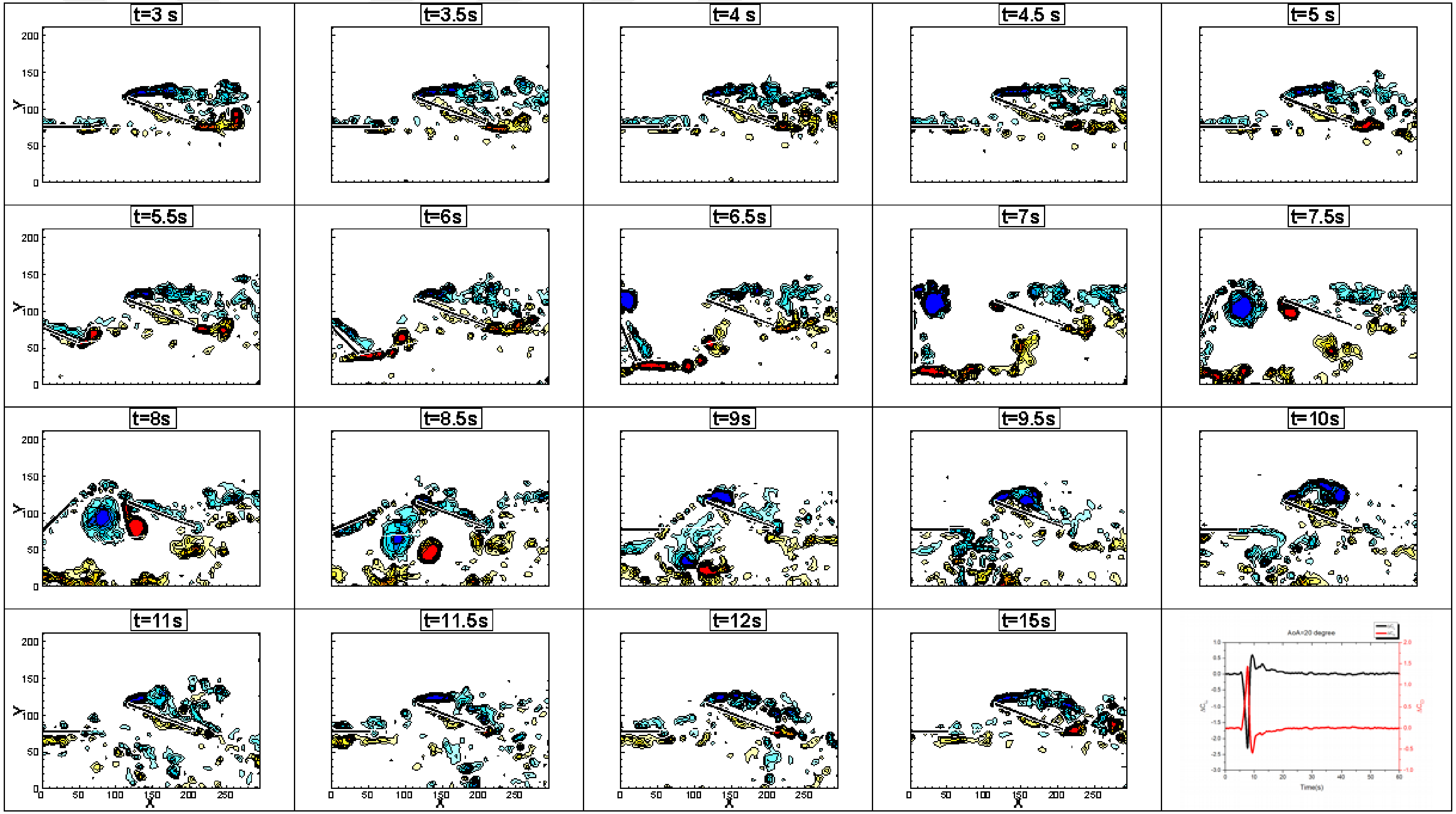

Figure A.15 Vortex Encounter DPIV Images for AoA=20 °, offset=39 mm

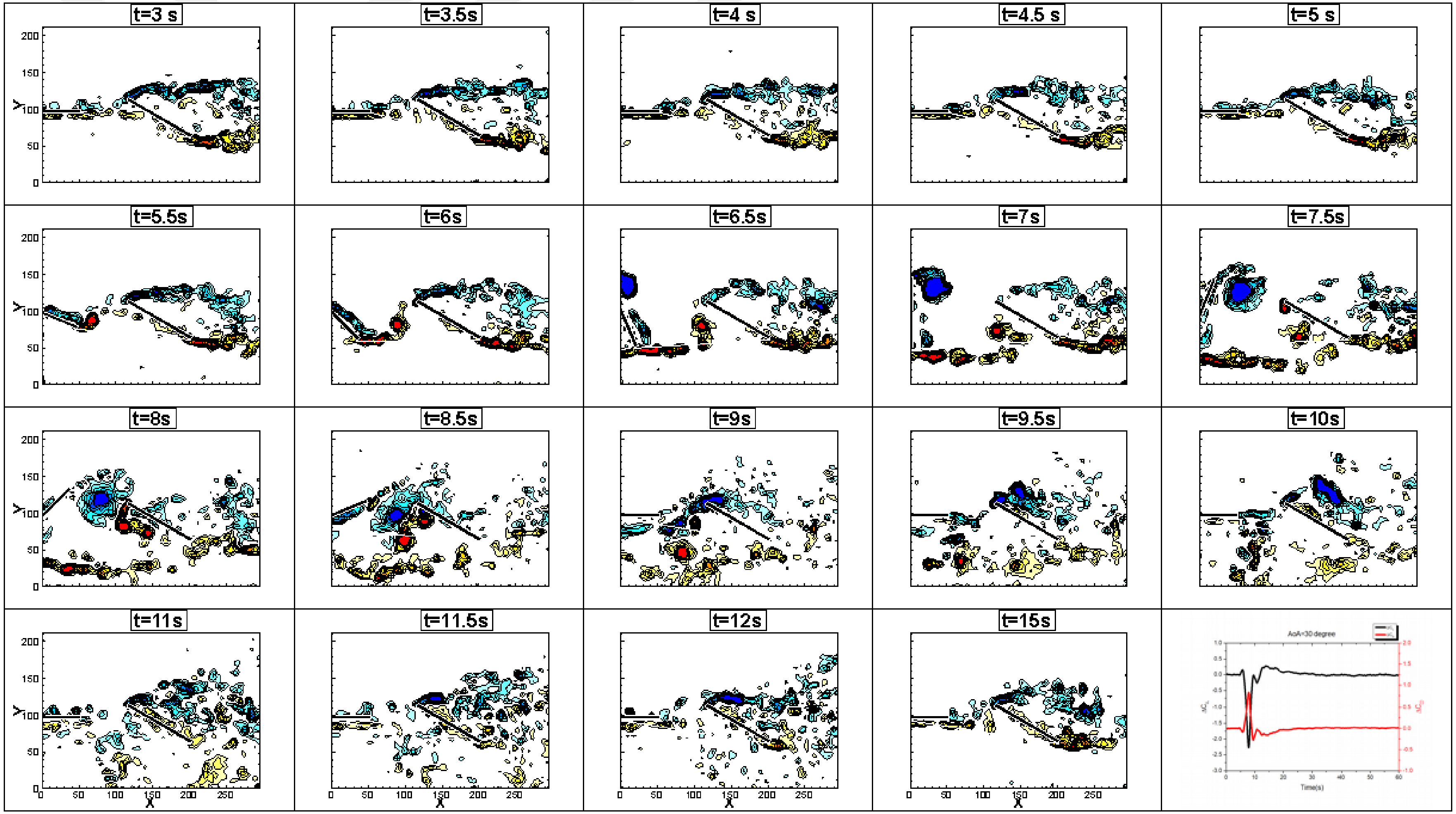

Figure A.16 Vortex Encounter DPIV Images for AoA=30 °, offset=19 mm

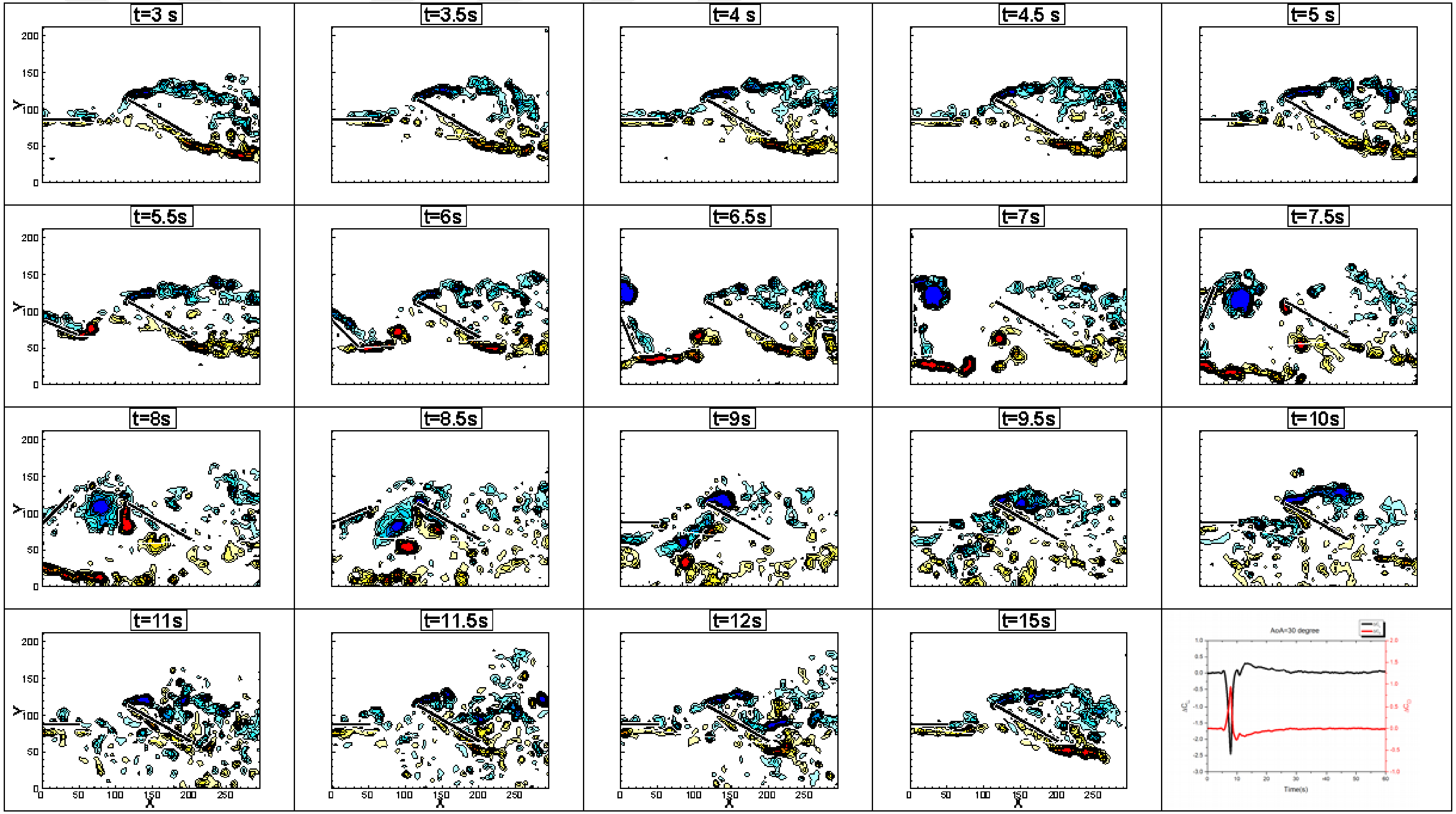

Figure A.17 Vortex Encounter DPIV Images for AoA=30 °, offset=29 mm

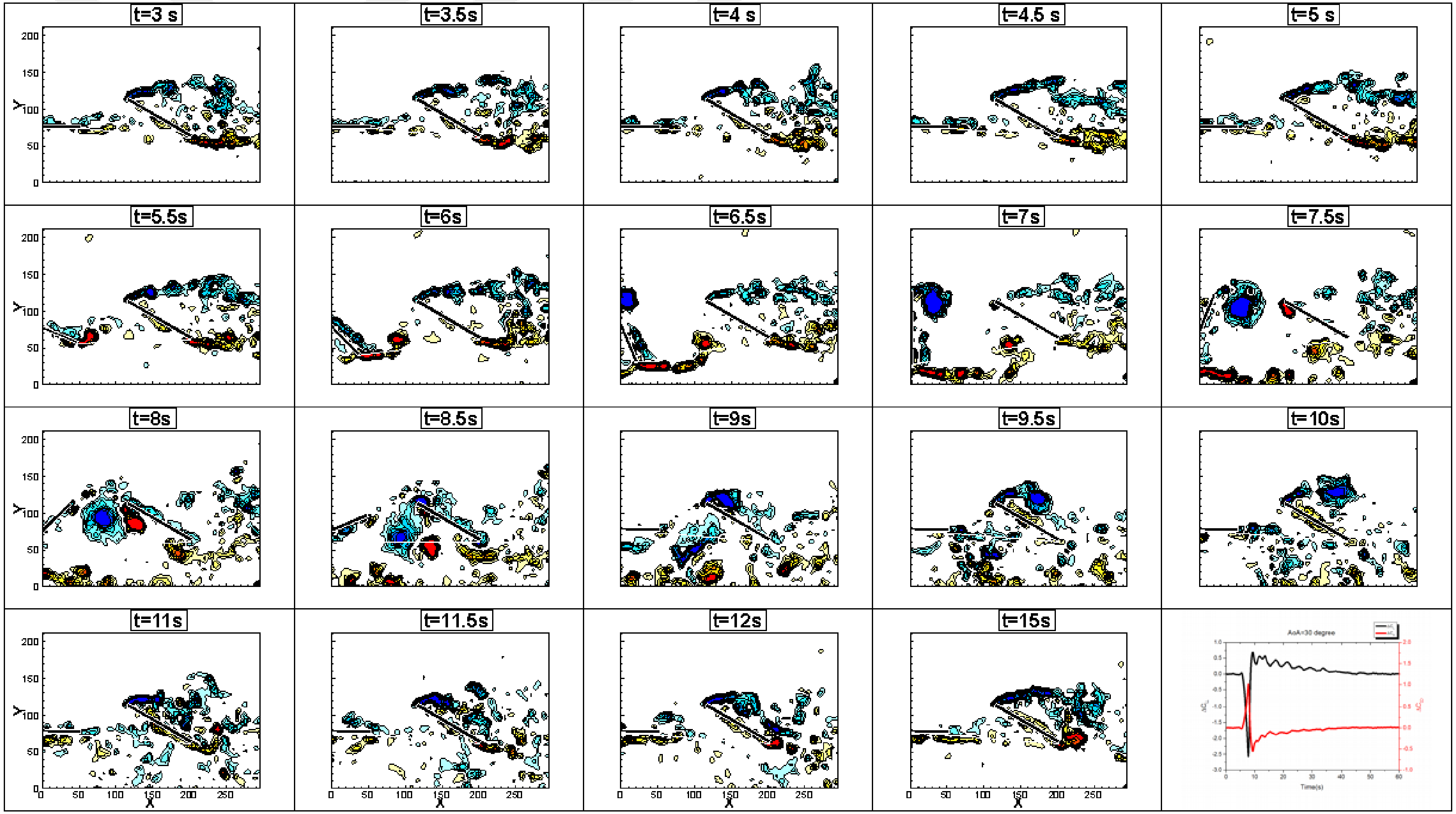

Figure A.18 Vortex Encounter DPIV Images for AoA=30 °, offset=39 mm

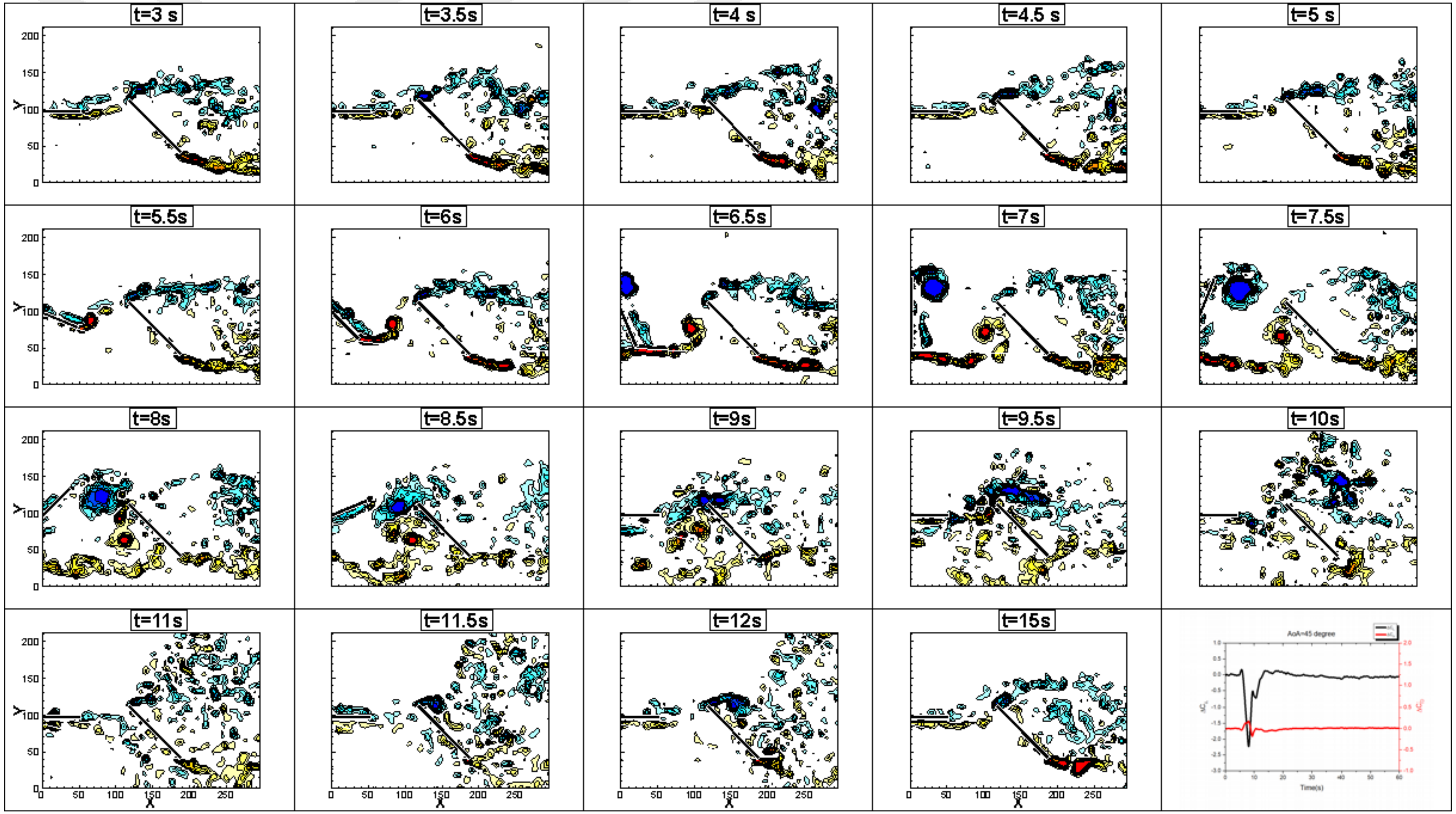

Figure A.19 Vortex Encounter DPIV Images for AoA=45 °, offset=19 mm

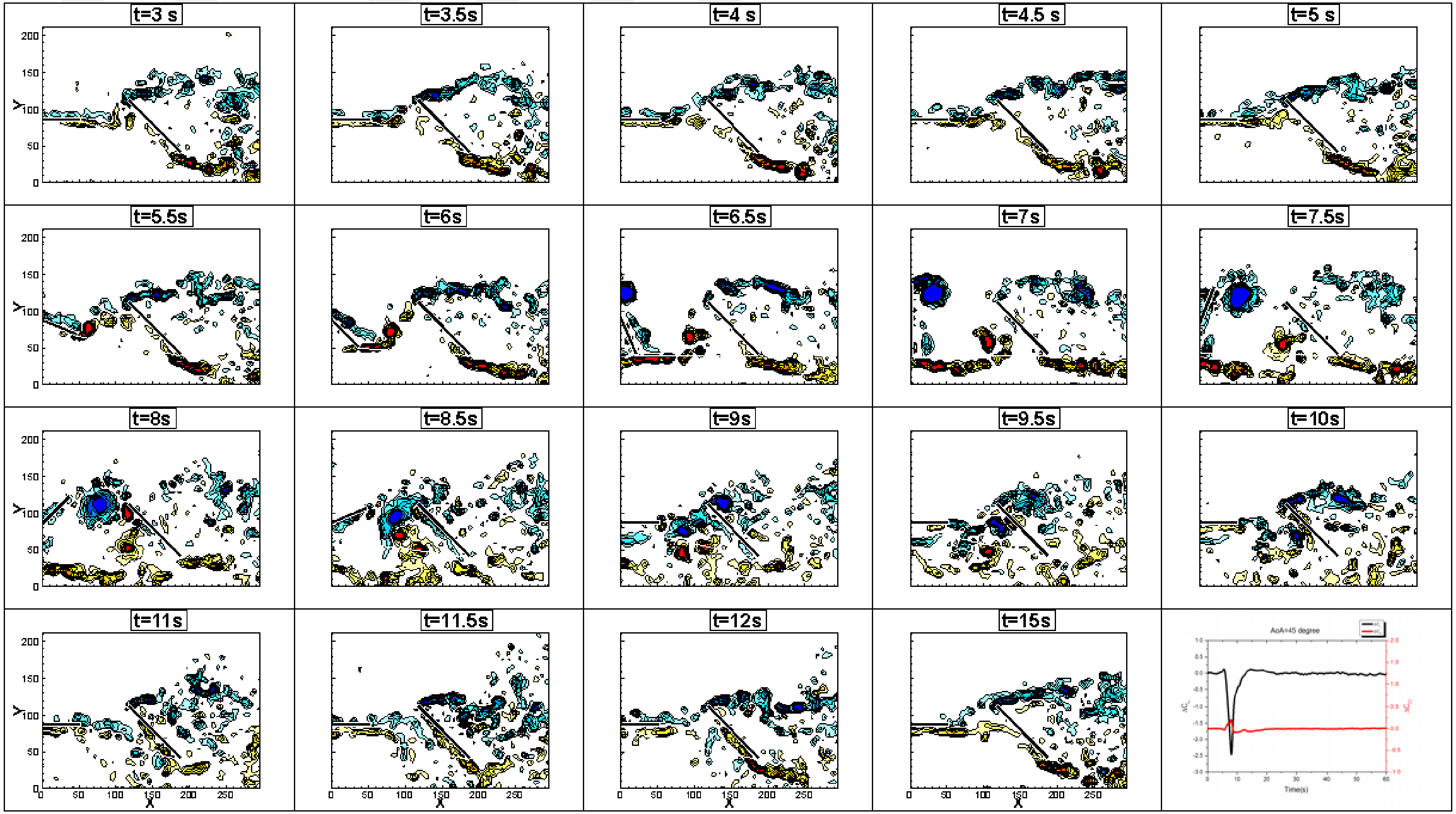

Figure A.20 Vortex Encounter DPIV Images for AoA=45 °, offset=29 mm

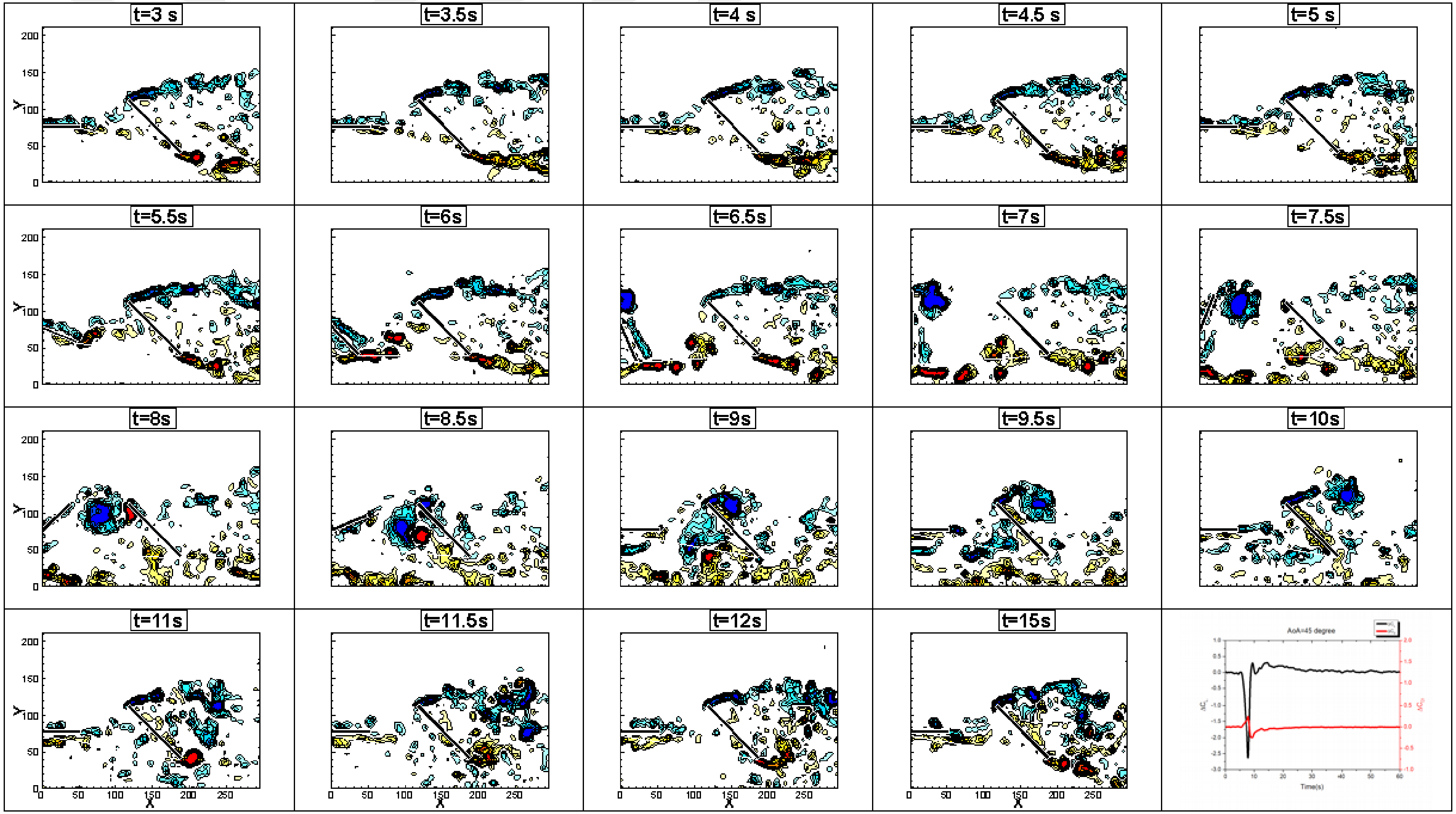

Figure A.21 Vortex Encounter DPIV Images for AoA=45 °, offset=39 mm

CURRICULUM VITAE

Name Surname **:** Kader Engin

Place and Date of Birth **:** İSTANBUL, 1994

E-Mail **:** enginka@itu.edu.tr

EDUCATION **:**

- **B.Sc.** **:** 2017, İTÜ, Faculty of Aeronautics and Astronautics, Astronautical Engineering Program

PROFESSIONAL EXPERIENCE AND REWARDS:

- **The performance of the flapping wings under the effect of gust and the flow control attempt for UAV and MAV application**, 2016-2018, Project Assistant

PUBLICATIONS, PRESENTATIONS AND PATENTS ON THE THESIS:

- **Kader Engin, Egemen Aydin, Berk Zaloglu, Idil Fenercioglu, Oksan Cetiner** (2018): Large Scale Spanwise Periodic Vortex Gusts or Single Spanwise Vortex Impinging on a Rectangular Wing. AIAA Aviation